Construction and Building Materials 351 (2022) 128356

Contents lists available at ScienceDirect

Construction and Building Materials

journal homepage: www.elsevier.com/locate/conbuildmat

Cyclic shear behaviour of masonry triplets with rubber joints

Prateek Kumar Dhir [a,*], Enrico Tubaldi [a], Alessandra Orfeo [a], Hamid Ahmadi [b]

[a] Department of Civil and Environmental Engineering, University of Strathclyde, Glasgow G11XQ, UK
[b] Tun Abdul Razak Research Centre (TARRC), Brickendonbury, Hertford SG13 8NL, UK

ARTICLE INFO

Keywords:
Masonry triplets
Monotonic shear
Cyclic shear
Rubber joints
Hysteretic behaviour

ABSTRACT

This paper presents the outcomes of an extensive experimental campaign and of numerical analyses aimed at characterising the cyclic shear behaviour of masonry triplets with mortar-rubber joints under both monotonic and cyclic loading. These joints consist of rubber strips placed between two mortar layers with the aim of enhancing the flexibility of masonry components while providing some auxiliary energy dissipation. The main application of the rubber joints is for enhancing the performance of masonry-infilled reinforced concrete frames under both in-plane and out-of-plane loading, thanks to a reduced interaction between the infill panels and the frame. Although past tests have investigated the behaviour of multi-layer flexible joints, no in-depth study has been carried out to date on the hysteretic and dissipative properties of mortar-rubber joints. In order to fill this gap, a series of experimental tests were conducted at the University of Strathclyde to characterise the mechanical behaviour of the various components of the rubber-masonry triplets as well as the behaviour of the composite system, with particular focus on the cyclic shear response and the bond strength. The hysteretic responses of the triplets obtained from the experiments are simulated using a micro-modelling strategy developed in Abaqus. The study results are useful for informing modelling strategies for the design and analysis of rubber joints, and for the selection of the most suitable mechanical and geometrical properties of these seismic protection devices.

1. Introduction

Past seismic events have revealed the significant vulnerability of masonry infilled reinforced concrete (RC) building frames and the large human and economic losses caused associated with this [1–4]. Masonry infills are often among the most critical components of infilled RC buildings. In fact, while columns and beams are designed to be earthquake-resistant, masonry infills are often disregarded in the design stage and considered as non-structural members. Therefore, even under minor earthquakes, infills undergo severe damage, causing injury or death of occupants and hindering rescue operations.

In the recent years, a promising approach has emerged to protect infill walls from seismic damage through the use of sliding joints [5–11] and flexible/soft layers [12–18] for increasing the flexibility of infill panels and isolating them from the surrounding frame. These layers can be horizontal, inserted between rows of bricks or between the panel and the top beam of the frame, or vertical, placed between the infill panel and the columns (Fig. 1a). The Tun Abdul Razak Research Centre (TARRC) has developed an innovative rubber joint (Fig. 1b) made from a high-damping natural rubber (HDNR) compound. The joint has a non-flat profile whose shape has been defined in order to achieve different stiffness in the in-plane and out-of-plane direction and improve the out-of-plane capacity of the infills by invoking an arching mechanism [13]. It does not require skilled labour to be deployed and is available in two versions (DRES-V1 and DRES-V2 [19]), which differ only for the presence of pins in the second one. These pins are introduced to enhance the bond between the rubber and the mortar and avoid sliding. In fact, even if sliding can be considered as an excellent mechanism for both reducing infill damage and dissipating energy through friction [6], it is not desirable since it does often result in residual displacements.

The European research project INSYSME [20] (INnovative SYStems for earthquake-resistant Masonry Enclosures in reinforced concrete buildings) has proven the effectiveness of the rubber joints during tests carried out on the seismic protection of infill walls. In particular, in-plane and out-of-plane quasi-static tests were carried out at University of Padova [19] on an infilled reinforced concrete frame with and without rubber joints. The tests demonstrated the “proof of concept” of the technology and showed that the introduction of the rubber joints considerably minimises the masonry infill damage and provides excellent out-of-plane performance in terms of stiffness and strength.

* Corresponding author.
E-mail address: prateek.dhir@strath.ac.uk (P.K. Dhir).

https://doi.org/10.1016/j.conbuildmat.2022.128356
Received 12 December 2021; Received in revised form 7 May 2022; Accepted 2 July 2022
Available online 6 September 2022

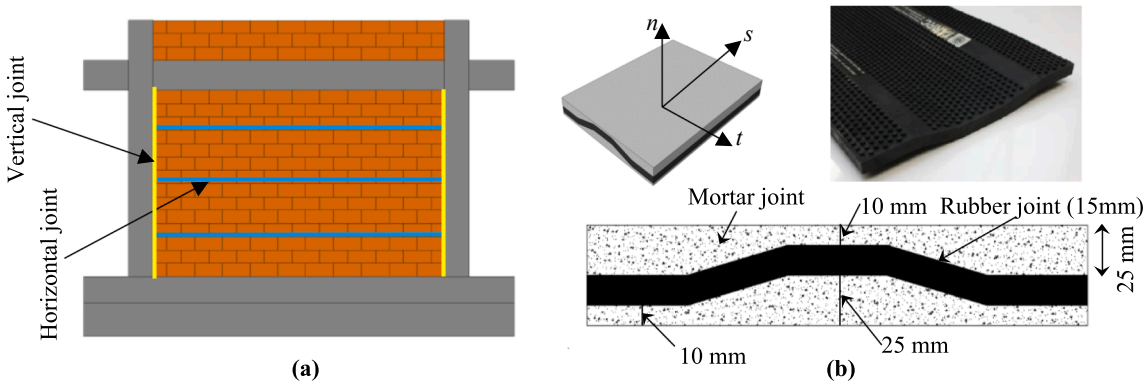

Fig. 1. (a) Masonry infilled walls with horizontal and vertical joints, (b) HDNR joint developed by TARRC.

Moreover, they showed that the rubber joints may contribute to increase the energy dissipation capabilities of the system, although this potential contribution was not investigated in depth.

Further experimental and numerical investigations are needed to fill this gap of knowledge in the dynamic behaviour of infilled frames with rubber joints. In particular, more experiments are needed to characterise the dissipation capabilities of the joints and of systems equipped with them, and the strength of the bond between the rubber joints and the mortar. Since the rubber joints introduce flexibility and dissipate the seismic energy by deforming in shear, a characterization of the cyclic shear behaviour of the HDNR compound and of the rubber-mortar joints is needed.

In order to fill this gap, an extensive experimental campaign was carried out at the University of Strathclyde. Material characterisation tests were performed to characterise the mechanical properties of bricks, mortar and HDNR. Moreover, an unconventional experimental setup was used to evaluate the cyclic shear behaviour of masonry triplets with mortar and rubber joints, rather than only the behaviour under monotonic loading as required by standards [21]. A similar test setup was recently developed and employed to characterise the shear behaviour of masonry triplets with multi-layer bed joints [14,22], dry stack masonry joints [23], and traditional mortar joints [24].

The results of the experimental investigation provide a better understanding of the mechanical properties of mortar-rubber joints. They are also useful to inform numerical studies aimed at characterising the dynamic behaviour of RC frames with masonry infill and rubber joints. On this regard, in the last decades numerous strategies have been developed for the analysis of traditional masonry infills, using macro models [25–33], micro models [34–36], discrete-element models [37], and mesoscale models [36,38–43]. Although some numerical studies have been carried out to evaluate the behaviour of masonry infill walls with soft or sliding joints [7,10,12,14,17], the case of rubber joints has not been fully investigated yet. Dhir et al. [44] has recently developed a modelling strategy in Abaqus for evaluating the in-plane quasi-static behaviour of RC frames with masonry infills and rubber joints, using a mesoscale approach. The results of the experimental campaign can be used to further expand this modelling strategy in order to investigate how the damping capabilities of the joints can effectively help reducing the seismic demand imposed on RC infilled frames. For this reason, the test results are simulated in this paper by using a detailed micro-modelling strategy, with the mechanical parameters of the constituent materials of the triplets informed by material tests on mortar, brick and rubber samples. The results of the experimental and numerical investigations of this study are useful for identifying research gaps in the understanding and description of the behaviour of mortar-rubber joints. They also inform future studies on the evaluation and analysis of the seismic performance of masonry infilled frames with rubber joints, and on the evaluation of optimal mechanical and geometrical properties of the rubber joint properties.

The rest of the paper is organised as follows; Section 2 describes the experimental campaign conducted to characterise the masonry unit, mortar and HDNR compound. Manufacturing and testing procedures of triplets with both mortar and mortar-rubber joints are also described in this section. Section 3 illustrates the simulation of the experimental tests described in Section 2 carried out using a micro-modelling approach, and Section 4 reports the conclusions of this study.

2. Experimental campaign

This section describes first the characterisation tests of the materials composing the masonry triplets, namely the bricks, the mortar and the HDNR compound. In the second part of the section, the cyclic test apparatus is described, and the monotonic and cyclic shear tests on the masonry triplets with traditional mortar joints and mortar-rubber joints are presented.

2.1. Brick and mortar characterisation

In this study, standard fired clay bricks (Birtley old English bricks) of dimensions 215 × 102.5 × 65 mm^3 were used. Although these bricks are only one of the many types of bricks and blocks employed in masonry infill wall construction, they were chosen because they were easy to get locally, and because the main aim of the study was to investigate the behaviour of the mortar-rubber joints. Nevertheless, it must be stressed that the typology of brick and mortar is important and should be carefully considered to guarantee a good shear bond at the brick–mortar interface, allowing the deformation of the rubber device. The bricks were tested under uniaxial compressive loading (0.1 mm/min) along the horizontal and vertical directions (Fig. 2a, c). The Young's modulus of bricks (E_b) was calculated from its stress–strain curves assuming a linear elastic response for compressive stresses between 5% and 33% of the peak strength (see Fig. 2b, d). A three-point bending test was also carried out on the brick units at a rate of 0.5 mm/min to estimate the flexural strength (Fig. 2e) and the load displacement relation is presented in Fig. 2f. The test results are summarised in Table 1.

General-purpose ready-mix mortar (Cement: Sand = 20–25%: 75–80%) was prepared with a water to cement ratio of 0.8:1.0 to ensure the easy workability. Flexural strength tests (Fig. 3) and cube compressive strength tests (Fig. 4) were conducted to characterise the mechanical properties of the mortar. Mortar specimens were left to cure at a temperature of about 25 °C for 28 days before being tested.

For the flexural strength tests of mortar, a total of 6 mortar beams of size 40 × 40 × 160 mm^3 were prepared and a three-point bending test was performed on the mortar beam specimens under a displacement rate of 0.5 mm/min [24]. The flexural strength, f_f of mortar specimens were found following EN [45] as follows:

$$f_f = \frac{3}{2}\frac{R_f l}{bh^2} \quad (1)$$

(a)

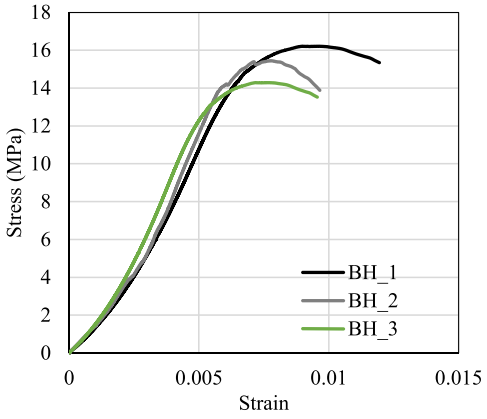

(b)

(c)

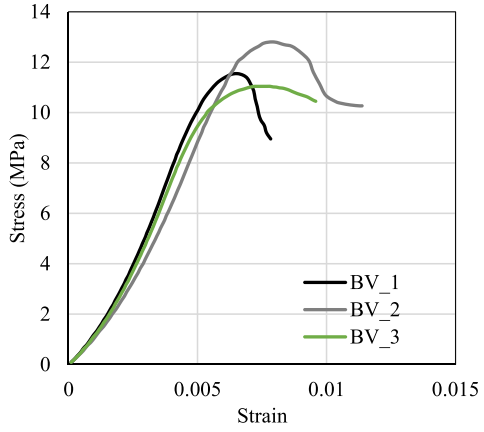

(d)

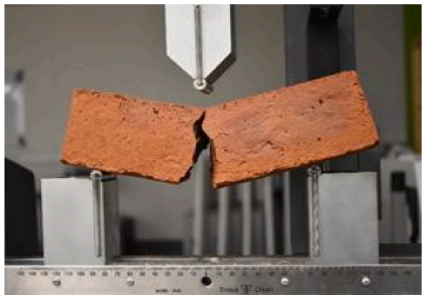

(e)

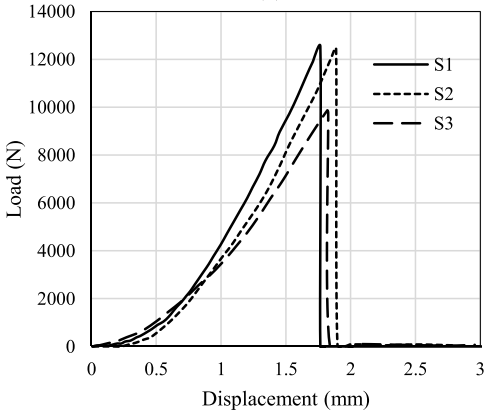

(f)

Fig. 2. (a, c) compressive strength test on bricks in horizontal and vertical direction, (b, d) stress–strain curves for bricks in horizontal and vertical direction, (e) test setup for three-point bending test of brick specimens, (f) load–displacement response of brick specimens under three-point bending.

where R_f is the failure load, l is the length between the two supports while testing, b and h are the width and height of the mortar specimen cross-section, respectively.

Similarly, a total of 6 mortar cubes of size 50 × 50 × 50 mm^3 were cast and subjected to compressive strength tests. The mortar cubes were tested on the 28th day since casting at a constant displacement rate of 0.1 mm/min [24]. Fig. 5a and b show the load–displacement curves obtained in the flexural and compression tests, respectively. The Young's modulus (E_m) of each mortar sample was calculated from compressive strength tests by assuming a linear elastic response for compressive stresses between 5% and 33% of the peak strength [24]. The strain values reported in abscissa refer to the ratio between the displacement of the loading plates and the total height of the specimen. Table 2 summarises the values of the mortar mechanical properties from the various tests as well as the average ones. The displacements reported are those measured by the loading machine. It is noteworthy that the compliance of the testing machine may lead to some inaccuracy in the estimate of the displacements. Local confinement effects near the loading plates may also affect the displacement estimates.

2.2. Characterisation of HDNR compound

The horizontal deformable joints are the core element of the proposed system. During the experimental campaign, DRES-V2 joints [19]

Table 1
Mechanical properties of clay brick specimens.

Three-point bending test				Compressive strength					
				Horizontal direction			Vertical direction		
Samples	Density (kg/m^3)	R_f [N]	f_f (MPa)	Samples	f_c (MPa)	E_b (MPa)	Samples	f_c (MPa)	E_b (MPa)
S1	1852	12,523	5.61	BH_1	16.2	20,125	BV_1	11.4	16,882
S2	1929	12,440	5.57	BH_2	15.2	19,493	BV_2	12.6	17,748
S3	1971	9774	4.38	BH_3	14.7	19,170	BV_3	11.1	16,658
Mean (CoV)	1918 (0.031)	11,579 (0.135)	5.19 (0.135)		15.37 (0.050)	19,596 (0.025)		11.7 (0.068)	17,096 (0.034)

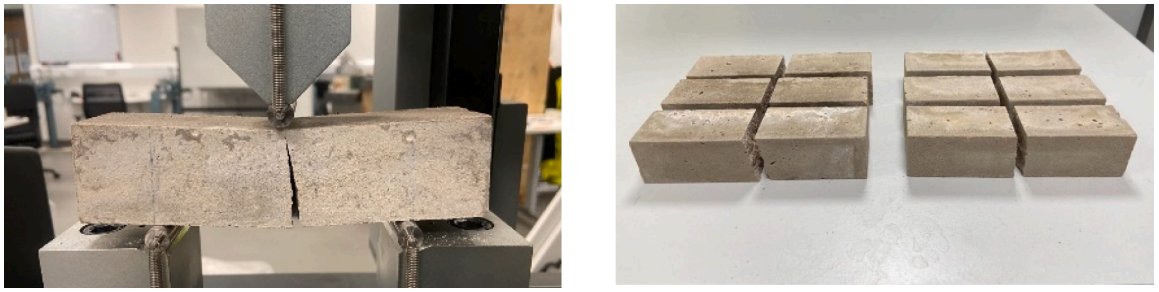

Fig. 3. (a) Three-point bending test of mortar beam (b) failed mortar beams.

Fig. 4. (a) Compressive-strength test of mortar cube, (b) failed mortar cube.

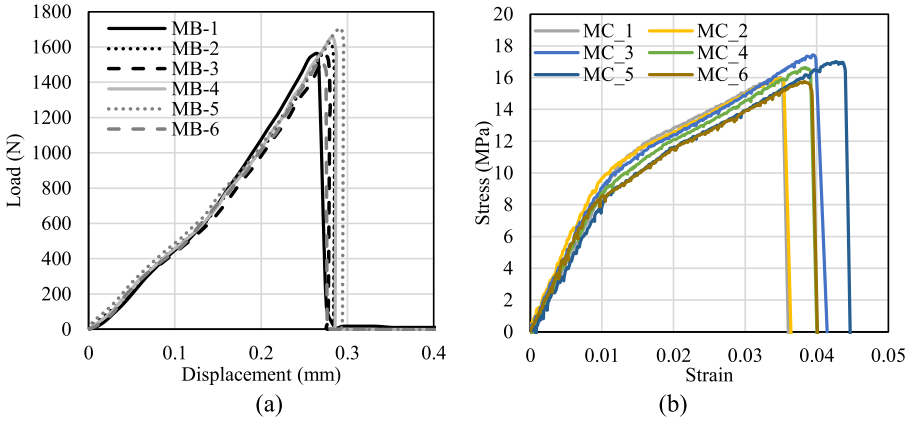

Fig. 5. (a) Three-point bending tests on mortar beams, (b) compression tests on mortar cubes.

Table 2
Mechanical properties of mortar specimens.

Three-point bending test				Compressive strength test		
Samples	Density (kg/m^3)	R_f [N]	f_f (MPa)	Samples	f_c (MPa)	E_m (MPa)
MB_1	2043	1556.18	3.65	MC_1	16.01	1780.87
MB_2	2094	1622.60	3.80	MC_2	15.95	1629.09
MB_3	2078	1547.13	3.63	MC_3	17.43	1875.38
MB_4	2063	1657.50	3.88	MC_4	16.64	1780.00
MB_5	2086	1706.73	4.00	MC_5	17.05	1832.10
MB_6	2070	1528.25	3.58	MC_6	15.74	1709.00
Mean	2072	1603.06	3.76	Mean	16.47	1767.74
(Cov)	(0.009)	(0.044)	(0.044)	(Cov)	(0.041)	(0.050)

(Fig. 1b) were used. These joints have 15 mm thickness, 300 mm width, and 500 mm length. In order to characterise the behaviour of the HDNR compound used for the joints, specimens with different dimensions were cut from the joints and tested in tension and shear.

A quasi-static tensile test, consists of a loading–unloading cycle, was performed on three rubber strips (150 mm length, 25 mm width and 15 mm thick) in a uniaxial testing machine (Tinius Olsen 25ST [46]) at a loading rate of 10 mm/min. Fig. 6a shows the schematic diagram for the test setup. Fig. 6b and Fig. 6c show the deformed shape of one of the three rubber specimens during and after the completion of the test. It can be seen that at the end of the test specimen was buckled, due to some viscous deformations that recovered in few minutes after the end of the tests. Fig. 7a shows the hysteretic responses of the three specimens during the loading and un-loading cycle, in terms of nominal tensile stress σ and strainε. These are defined as follows:

$$\sigma = \frac{F_t}{b_w t_w} \tag{2}$$

$$\varepsilon = \frac{\delta}{l_0} \tag{3}$$

where $b_w t_w$ denotes the nominal (i.e. initial) cross-section area of the test piece, and l_0 the initial length, F_t is the tensile force, and δ is the displacement.

The responses of the three specimens are very close to each other. Fig. 7b shows the results of the relaxation phenomenon which is linear with log of time were carried out on a specimen. These were performed by pulling the specimen at an initial rate of 10 mm/min up to 100% and 200% of its length and holding it in this position for 24 h while measuring the change of resisting force. During the first seconds of hold

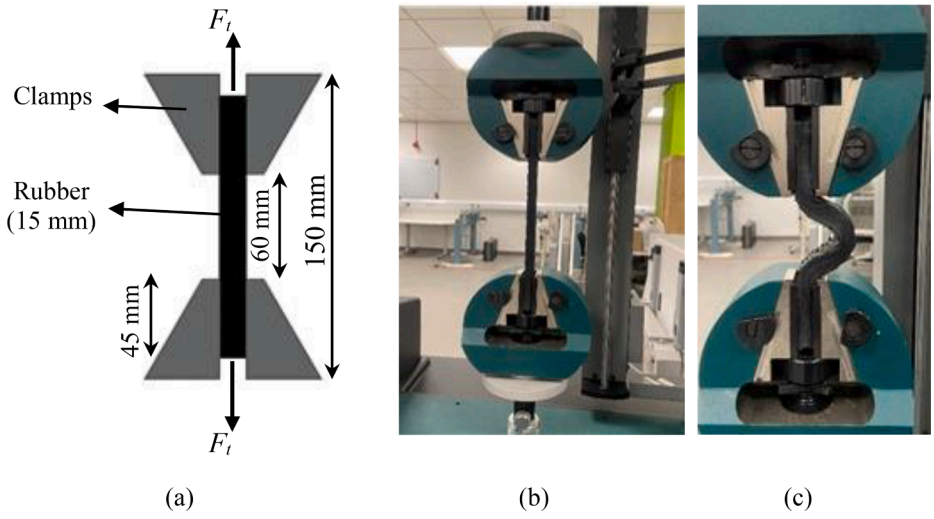

Fig. 6. (a) Tensile test setup of rubber strip, (b) deformed shape of the test piece during testing, and (c) at the end of the test.

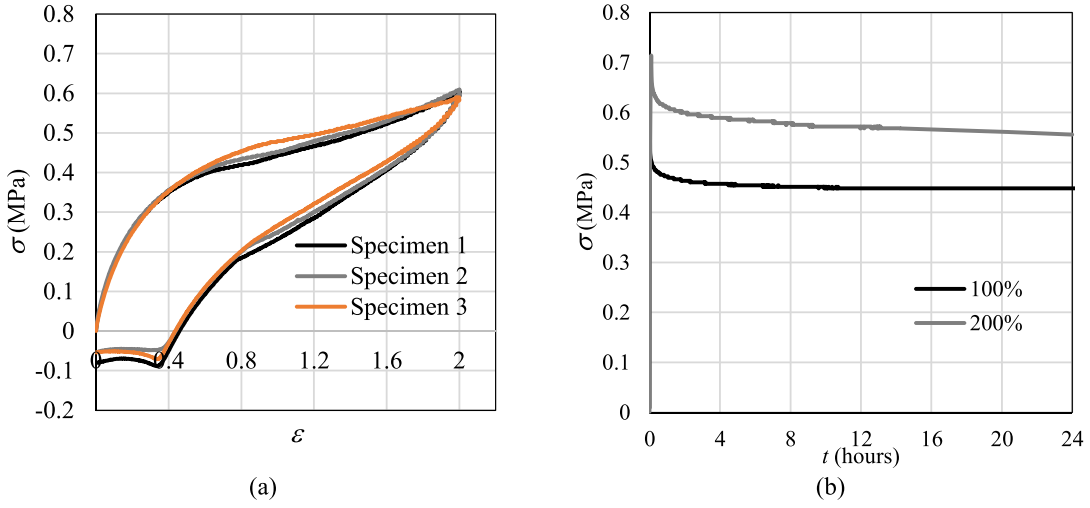

Fig. 7. (a) Tensile stress- strain response, and (b) relaxation test of rubber specimen.

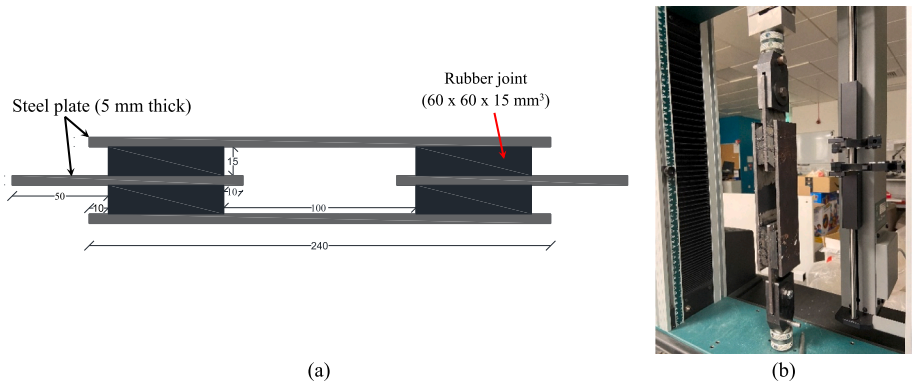

Fig. 8. (a) Quadruple test specimen, (b) Test setup.

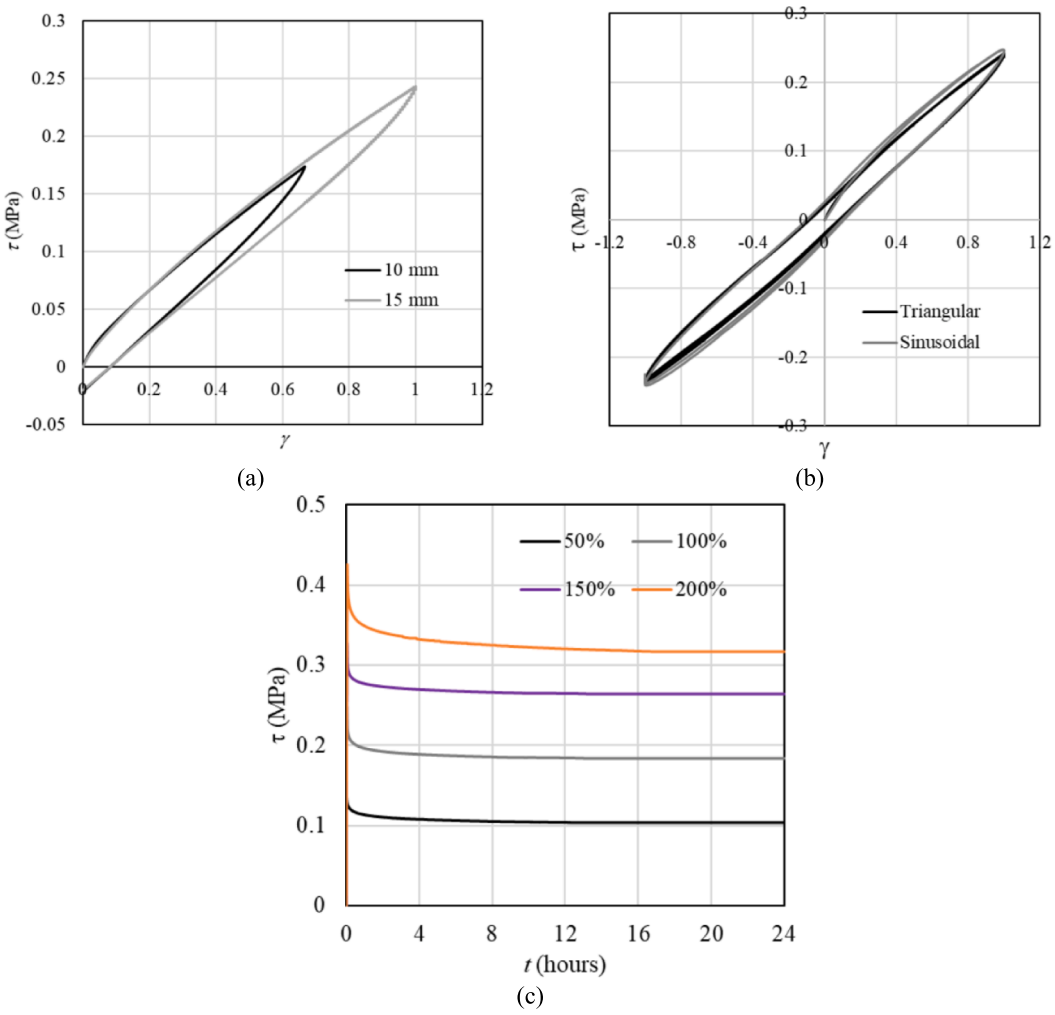

Fig. 9. Shear stress–strain response for (a) half displacement cycle at constant rate (b) full cycle, (c) relaxation test on rubber quadruplet for different initial strain amplitudes.

time, a very rapid decrease in the stress is observed. Subsequently, the rate of decrease reduces. In the case of 100% initial amplitude, it takes about 12 h before a constant asymptotic value can be assumed to be reached. After 12 h, the change of stress in the subsequent 12 h is less than 1% of the stress value at 12 h. In the case of 200% initial amplitude, a longer relaxation time (>24 h) is required to reach the asymptotic value.

In order to study the behaviour of the rubber compound under simple shear, which is the main mode of deformation of the horizontal joints under in-plane loading of the infilled frame, multiple quadruple specimens were prepared (Fig. 8a). Each specimen was made by gluing four rubber pieces (60 mm × 60 mm × 15 mm) to steel plates of 5 mm thick and Fig. 8b shows the testing setup of the rubber quadruplet tested at a rate of 10 mm/min. Plotted in Fig. 9a is the nominal shear stress–strain response of one quadruple specimen at different amplitudes of loading cycles. The results obtained with the other specimens are not plotted

because they are very close to each other. The nominal shear stresses and strains were obtained as follows:

$$\tau = \frac{F_s}{2A_s} \tag{4}$$

$$\gamma = \frac{u}{t_r} \tag{5}$$

where τ is the nominal shear stress, F_s = shear force, A_s = shear area of single block, γ= the nominal shear strain, u = shear displacement, t_r = thickness of block.

Relaxation tests were performed on the rubber quadruplets under shear by imposing 50%, 100%, 150% and 200% strain amplitudes. Each specimen was pulled at a rate of 10 mm/min and hold for 24 h. The results of the tests carried out on one specimen are plotted in Fig. 9c. Similar to the tensile test, after the initial seconds of hold time, a very rapid decrease in stress is observed and after 12 h, the change of stress in the subsequent 12 h is less than 1% of the stress value at 12 h, corresponding to the attainment of an asymptotic value.

The behaviour of rubber in simple shear is very complex, since it is rate-dependent, amplitude-dependent, and characterised by the Mullins effect [47]. In order to further investigate the dependency of the behaviour of the rubber joint on the displacement history and rate, another test was carried out on the quadruplets by imposing a sinusoidal displacement input with frequency 0.008 Hz and amplitude 15 mm. The corresponding hysteretic response obtained for a quadruplet is plotted in Fig. 9b and is quite similar to the one obtained with a constant-rate input of 10 mm/min. It is noteworthy that the frequency of the sinusoidal input is the same as that considered for the triplet tests presented below.

The secant shear modulus of the rubber (G_{eff}) and equivalent damping ratio (ξ_{eq}), evaluated considering the sinusoidal displacement input (γ=1), are equal to 0.25 MPa and 6% respectively. The secant shear modulus G_{eff} is obtained by dividing the values of the average shear stresses in the rubber by the values of the average shear strains corresponding to the maximum shear displacement level investigated. The equivalent damping ratio is defined as follows:

$$\zeta_{eq} = \frac{W}{4\pi E_{el}} \tag{6}$$

where W denotes the energy dissipated in one cycle (i.e. the area enclosed in the shear stress-strain hysteresis loop), $E_{el} = 1/2G_{eff}\gamma^2$ (elastic strain energy corresponding to the maximum deformation, γ).

2.3. Manufacturing of masonry triplets and test set-up

The clay brick triplets were prepared by bonding the bricks (see Fig. 10) with the ready-mix cement mortar. 42 triplets were prepared, 12 of which with mortar joints and 30 with mortar-rubber joints. The masonry triplets with mortar joints (10 mm thick) only were casted (Fig. 10a and c). The other triplets were prepared with mortar-rubber joints, with the rubber layers sandwiched between two layers of 10 mm thick mortar (Fig. 10b and d). Prior to assembling the triplets, all bricks were submerged in water for a minimum time of 24 h with the aim to improve their bonding with the mortar joints. After casting of triplets, they were left in the laboratory to cure for at least 28 days at a temperature of about 25 °C.

In order to characterise the cyclic behaviour of the triplets, the shear test set-up proposed by the European Standard EN [21] was modified and expanded (Fig. 11) in order to allow applying cyclic shear loadings. The developed apparatus is similar to the ones already employed in recent studies on the characterisation of the cyclic behaviour of masonry triplets with mortar joints [24,48,49], dry joints [23,50], and multi-layer bed joints [14,22].

Fig. 12 describes the assembly of the testing apparatus and the various components. A hydraulic jack is used to apply the pre-compression on the triplets in the horizontal direction. The pressure is applied before the shearing displacement, and it is kept constant during the entire duration of the test. The shearing vertical displacement is applied through a computer-controlled actuator (Fig. 11a) with a maximum load capacity of 250 kN. Both the monotonic and cyclic shearing test was performed on for three levels of pre-compressions (0.2

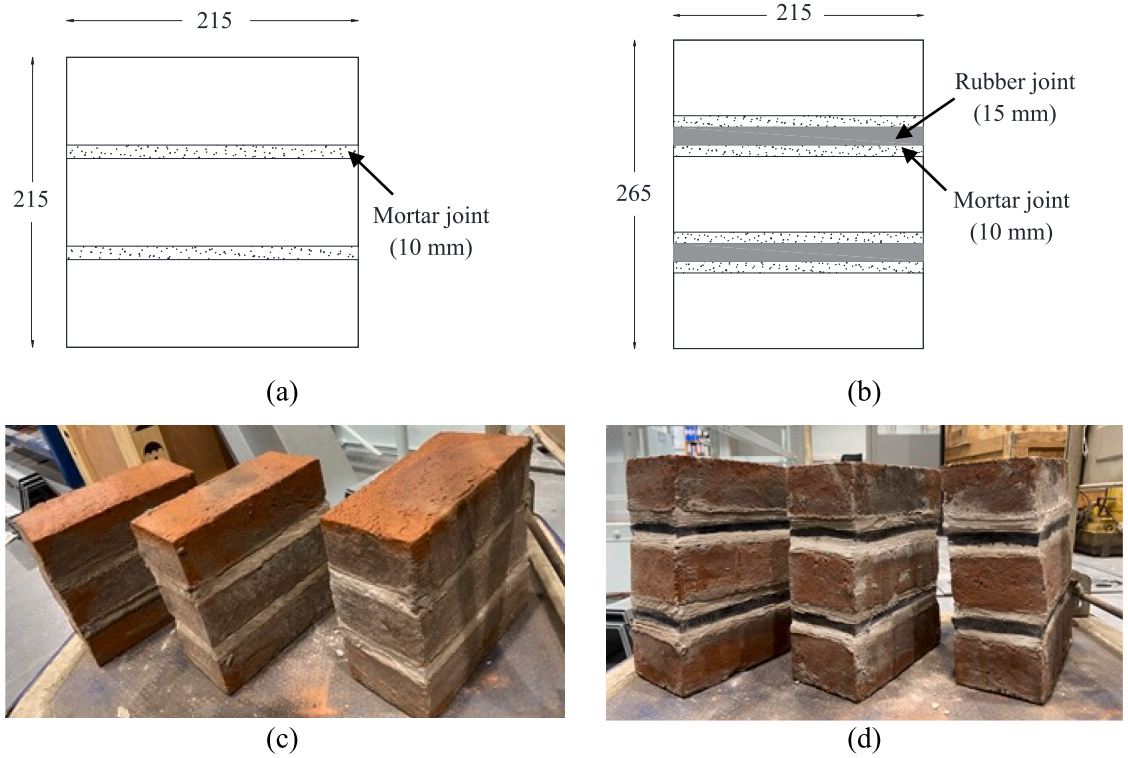

Fig. 10. (a, b) dimensions of the triplets with mortar and mortar-rubber joints, (c) triplet with mortar joint, (d) triplets with mortar-rubber joints.

MPa, 0.4 MPa and 0.6 MPa).

2.4. Monotonic and cyclic shear tests of triplets

The monotonic test was carried out by imposing a constant downward displacement rate of 1.0 mm/min on the intermediate brick through the actuator. The cyclic test was carried out by imposing downward and upward displacements over five sinusoidal cycles (frequency of 0.008 Hz). Fig. 13 shows the load–displacement relationship of the triplets with mortar joints under monotonic (Fig. 13a) and cyclic shear (Fig. 13b). The monotonic tests result show that the initial stiffness of the system is not affected by the pre-compression level, while the peak load increases for increasing pre-compression level. In the cyclic tests, lower force levels were obtained compared to the monotonic tests.

Fig. 14 show the failed specimens at the end of the monotonic and cyclic tests carried out at different levels of pre-compression. It can be seen from these results that the failure occurred at the mortar-brick joint interface, which was found to be weaker than the mortar layers and the bricks. The value of the cohesion and friction angle for the mortar joints (respectively 0.6 and 1.04), obtained with a mortar made with cement to sand ratio of 1:3–1:4, could be compared to those obtained by Barattucci et al. [24] (respectively 0.932 and 1.04) with a mortar made with cement to sand ratio of 1:3.

The triplets with rubber-mortar joints were tested under both monotonic loading (displacement rate 1 mm/min) and cyclic shear harmonic loading (frequency of 0.008 Hz). Fig. 15a shows a triplet during cyclic shear test. It can be seen that the rubber layer undergoes significant shear deformation, as expected. Fig. 15b shows the failed triplet at the end of testing. The rubber-mortar interface was found to be the weakest component in the system for all the investigated triplets. It is noteworthy that two or three tests were carried out on different triplets under the same loading condition in order to verify the repeatability of the results. Very similar responses were obtained with different specimens.

Fig. 16a shows the load–displacement response of the triplets with mortar-rubber joints under monotonic shear loading. Compared to the triplets with mortar joints (Fig. 13a), the triplets with mortar-rubber joints exhibit significantly lower stiffness (about 1/10), lower peak

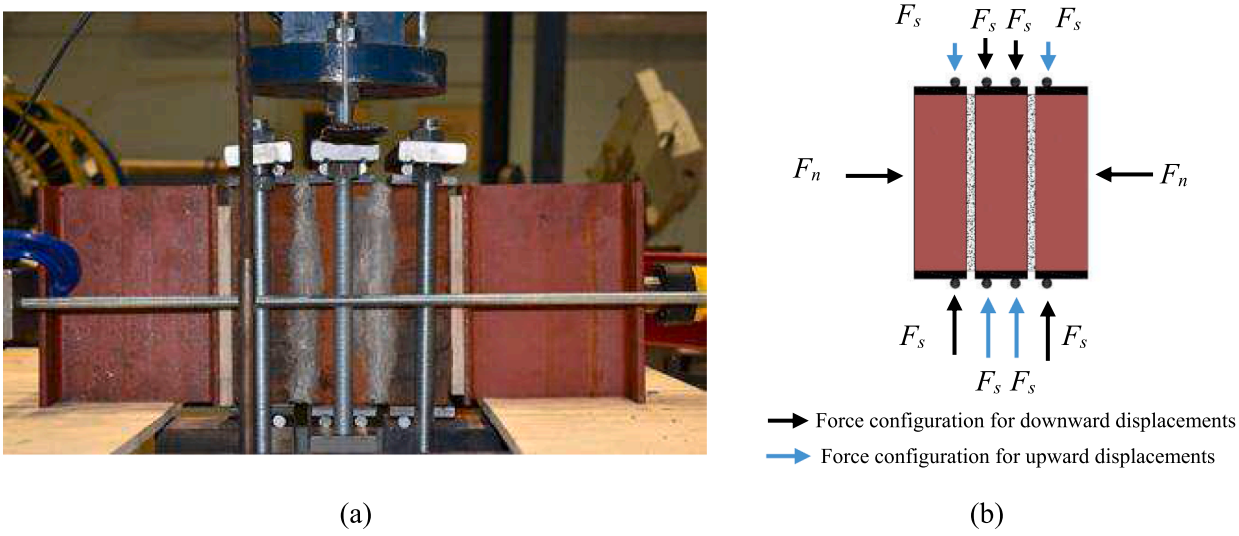

Fig. 11. (a) Shear test set-up, (b) forces configuration for cyclic shear test.

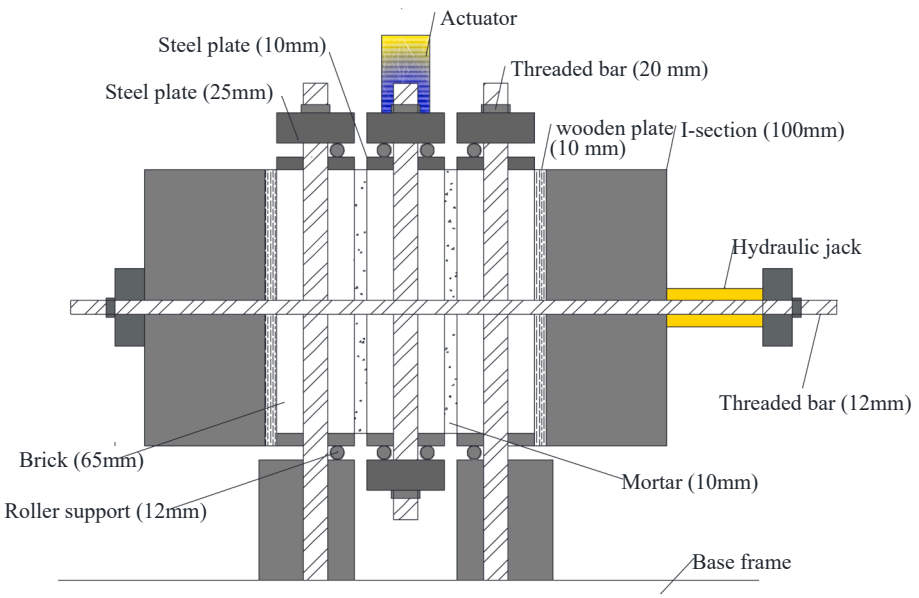

Fig. 12. Illustration of the components of the testing equipment apparatus.

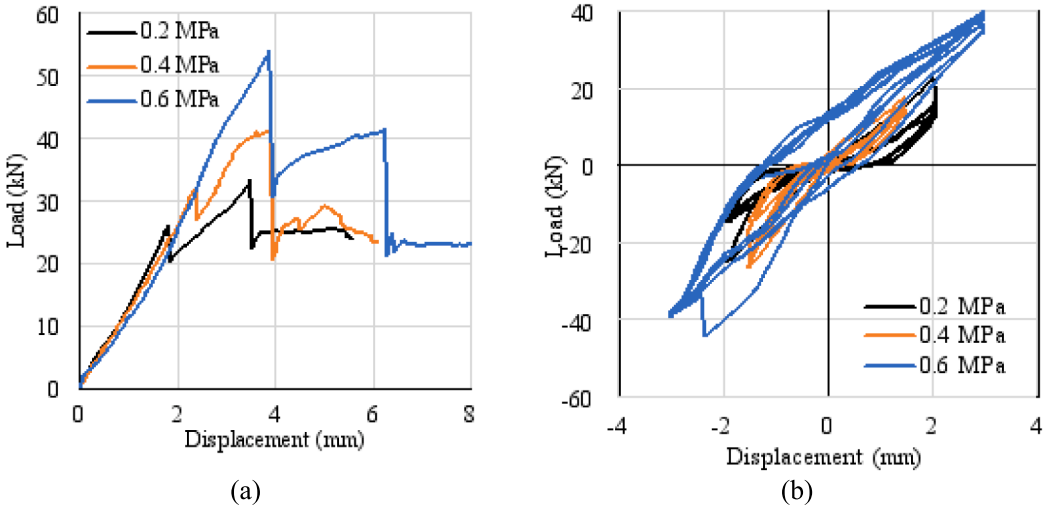

Fig. 13. (a) Monotonic, (b) Cyclic shear response of triplets with mortar joints.

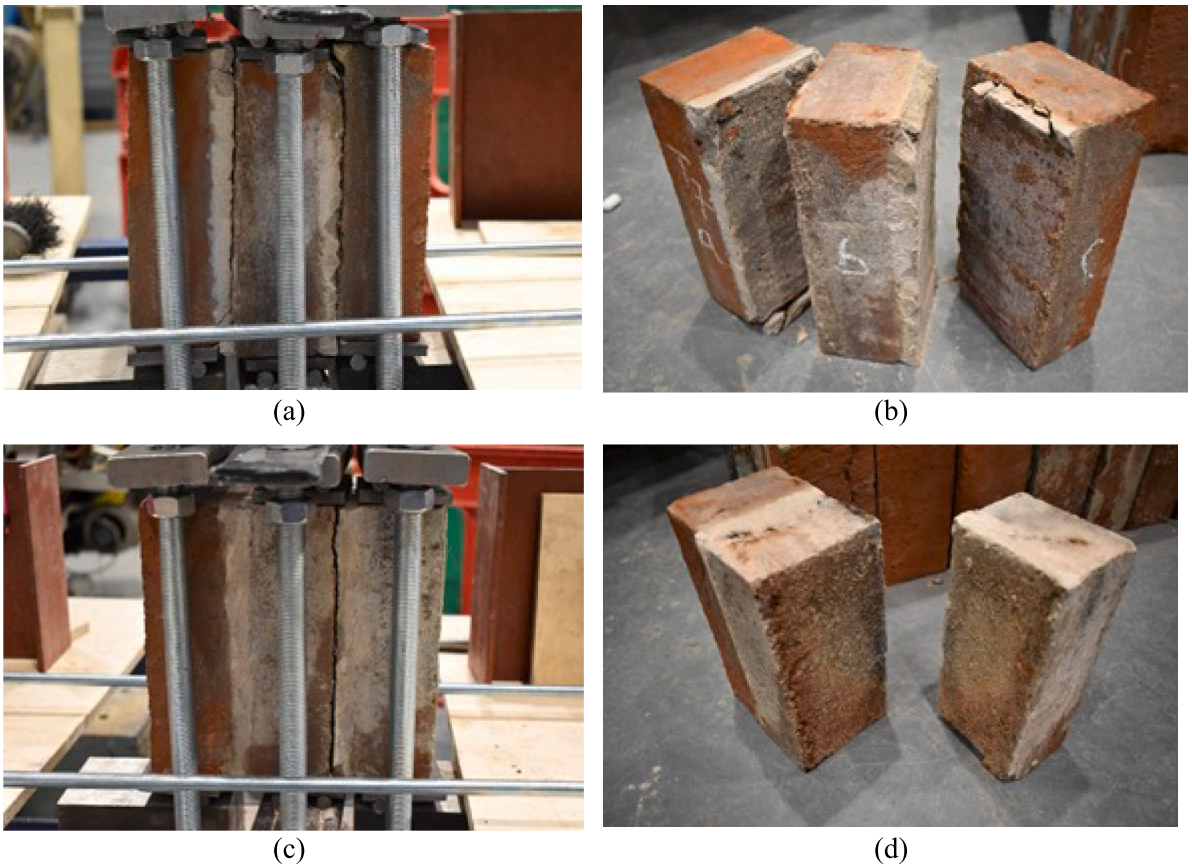

Fig. 14. (a, b) Monotonic, (c, d) Cyclic shear test of mortar triplets with 0.6 MPa pre-compression.

load capacity (about 1/5), and a less brittle post-peak response. The relatively weak bond between the joints and the mortar is responsible for the lower peak strength of the system. Nevertheless, the reduction of shear stiffness due to the rubber joint compliance is an important and useful feature of the mechanical behaviour of mortar-rubber joints, since it allows to increase the flexibility of masonry infills and to reduce the interaction between the infill and the frame while reducing the forces induced by the earthquake in the system for a given seismic drift demand. Fig. 16b-d show the cyclic shear response of the triplets with mortar-rubber joints obtained for different levels of pre-compression and different maximum displacement amplitudes. For each test, the results obtained with one of the many tested specimens are reported due to space constraints and to allow the comparison between tests. However, in Section 3 the results obtained with multiple tests under the same conditions are shown. It can be observed that the stiffness of the system increases slightly for increasing levels of pre-compression, whereas the dissipated energy does not change significantly. Quite surprisingly, significantly higher forces were attained in the cyclic tests without

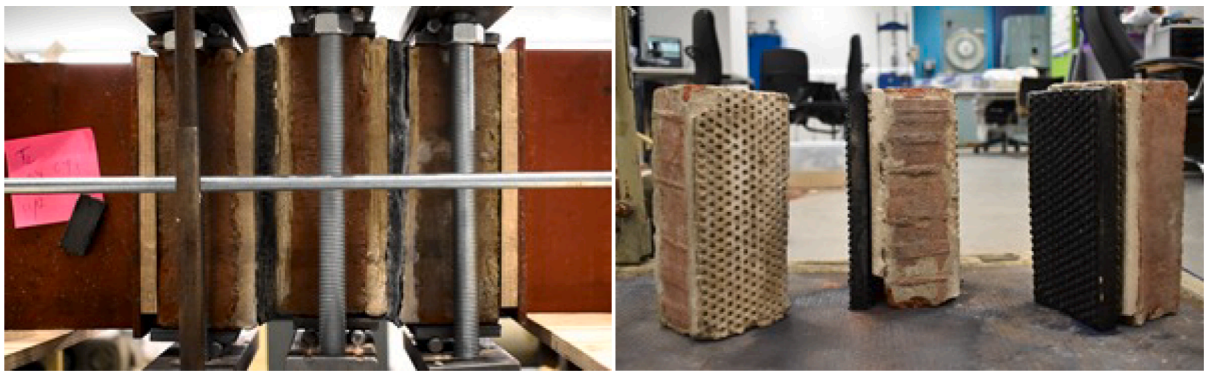

(a) (b)

Fig. 15. (a) Cyclic shear test setup, (b) failed specimens.

noting a complete failure of the bond compared to the monotonic tests and only in the case of low pre-compression level significant sliding at the mortar-joint interface was observed for high displacement amplitudes (i.e. 30 mm). A similar observation was made by Mojsilovic et al. [14], who observed an increased cohesion and an increase friction in cyclic tests compared to monotonic tests for mortar joints with interposed soft layers.

However, it should be noted that some sliding and energy dissipation due to friction is activated also for displacement amplitudes lower than 30 mm. This explains why the equivalent damping ratio measured with the triplet tests (discussed below, see Fig. 17b) is higher than the one measured with the quadruplet tests (Fig. 9b). The failure of the rubber-mortar interface for low levels of compression forces can potentially constitute a problem as it might limit the efficiency of the device and change the functioning mechanism, with the sliding at the rubber-mortar interface occurring in place of the rubber deformation. This could have consequences in terms of residual displacements at the end of the earthquake.

In order to better describe the effect of the pre-compression level and amplitude of oscillation on the hysteretic behaviour of the system, Fig. 17 shows the variation of the secant shear modulus of the rubber (G_{eff}) and equivalent damping ratio (ξ_{eq}) for increasing average shear strains and for different pre-compression levels. G_{eff} and ξ_{eq} are slightly affected by the pre-compression level, whereas they are strongly affected by the amplitude of shear deflection. In fact, G_{eff} reduces significantly with the amplitude of shear strain, whereas ξ_{eq} increases.

Overall, the rubber-mortar joints exhibit very good dissipative properties, with high values of the equivalent damping ratio that are significantly higher than those characteristics of the rubber compound. In fact, under a shear strain amplitude of 1, $\xi_{eq} = 6\%$ (measured through the quadruplet tests) whereas the rubber-mortar layer has ξ_{eq} in the range between 18% and 30%. The higher values of ξ_{eq} in the triplets can be due to the energy dissipation by friction that takes place at the interface between the mortar and the joints. This mechanism is enhanced by the presence of the pins in the rubber layers. It is noteworthy that these pins were removed before bonding the rubber to the steel plates to manufacture the quadruple test pieces. The friction between the pins and the surrounding mortar must be activated under small amplitudes, even when no significant sliding can be noticed.

Fig. 18 shows the cyclic shear response obtained for different frequencies of oscillation. It can be seen that the stiffness of the mortar-rubber joint and the energy dissipation capacity are not significantly affected by the frequency. It is noteworthy that it was not possible to test higher frequencies, which may be more representative of those characteristics of earthquake response of RC buildings with infills (i.e. higher than 1.0 Hz).

Table 3 reports the both peak loads of the masonry triplets exhibited in both the monotonic tests and the cyclic tests, for different levels of pre-compression. As already discussed, these values correspond to the rubber-mortar bond failure only in the case of monotonic loading.

Fig. 19 illustrates the relationship between the peak shear strengths, calculated as the ratio between the peak shear strength and two times the cross-sectional area of the interface, and the pre-compression stress, for the two types of triplets under monotonic loading. The peak shear strength for the three selected levels of pre-compression can be interpolated with a straight line, representing the Mohr-Coulomb failure criterion. This is expressed as:

$$\tau = c + \sigma_p \tan(\phi) \tag{7}$$

where σ_p is the pre-compression, c is the cohesion, and ϕ is the friction angle. Table 3 shows the values of cohesion and friction angle providing the best fit of Eq.2 to the experimental data. It can be seen that these values of the parameters provide a very good fit to the test results. In general, the capacity of the mortar joint is 4–5 times higher than that of the mortar-rubber joint, due to the relatively weak bond between the rubber and the mortar. The values of the cohesion and friction obtained for the mortar-rubber joints are comparable to those obtained experimentally by Verlato [19] with triplets made with the specially shaped DRES-V2 joints of Fig. 1b (c=0.12 MPa, $\tan(\phi)$=0.36).

3. Simulation of experimental tests

This section illustrates the simulation of the experimental tests described in Section 2 carried out in the commercial FE software Abaqus [51] using a micro-modelling approach [52].

3.1. Simulation of experimental tests on triplets with mortar joints

The two components of the triplets (bricks and mortar layers) are described as a continuum, and discretised using 3D 8-noded solid elements of reduced integration with hourglass control (C3D8R). The behaviour of the mortar and the brick units is described using a Concrete Damage Plasticity (CDP) model [53,54]. Surface-to-surface contact interfaces are used to simulate the bond between the mortar layers. The cohesive interfaces exhibit initially a linear elastic response, followed by a cracking behaviour that describes the most critical failure modes, namely, tensile cracking and shear sliding. This allows simulating the failure occurred in correspondence of the brick–mortar interfaces for the mortar triplets. Table 4 and Table 5 illustrate the main parameters

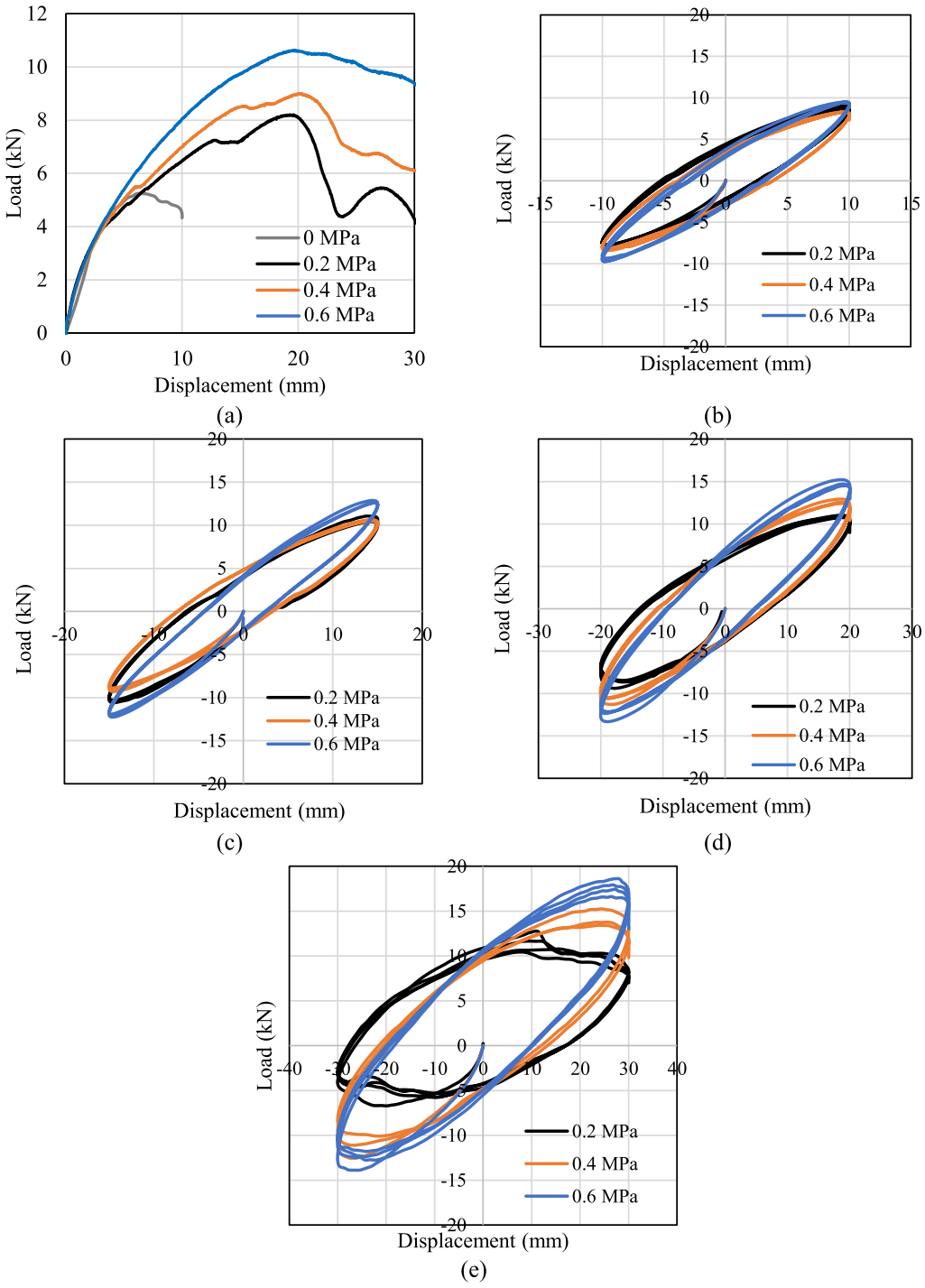

Fig. 16. Shear response of triplets with mortar-rubber joints for various levels of pre-compressions: monotonic loading (a) and cyclic loading (b, c, d, e).

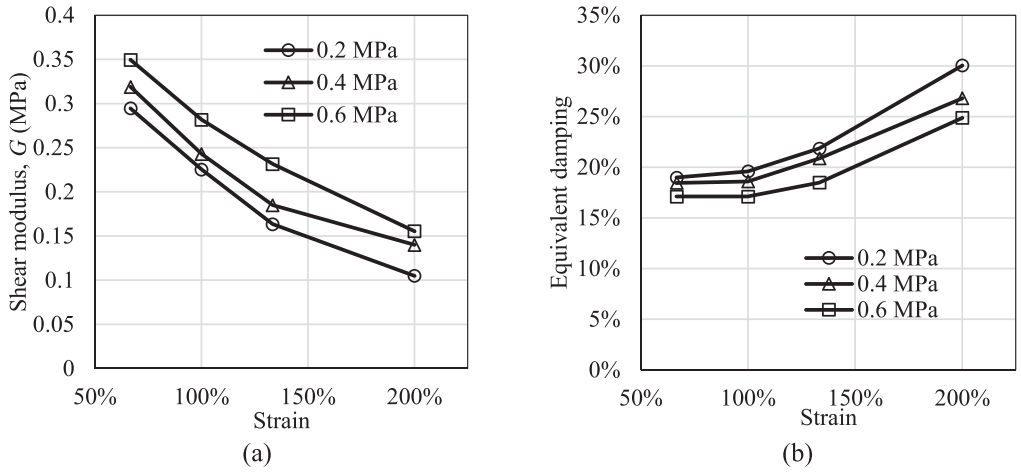

Fig. 17. Variation of the (a) secant shear modulus (b) equivalent damping with increasing shear strain at different compression levels.

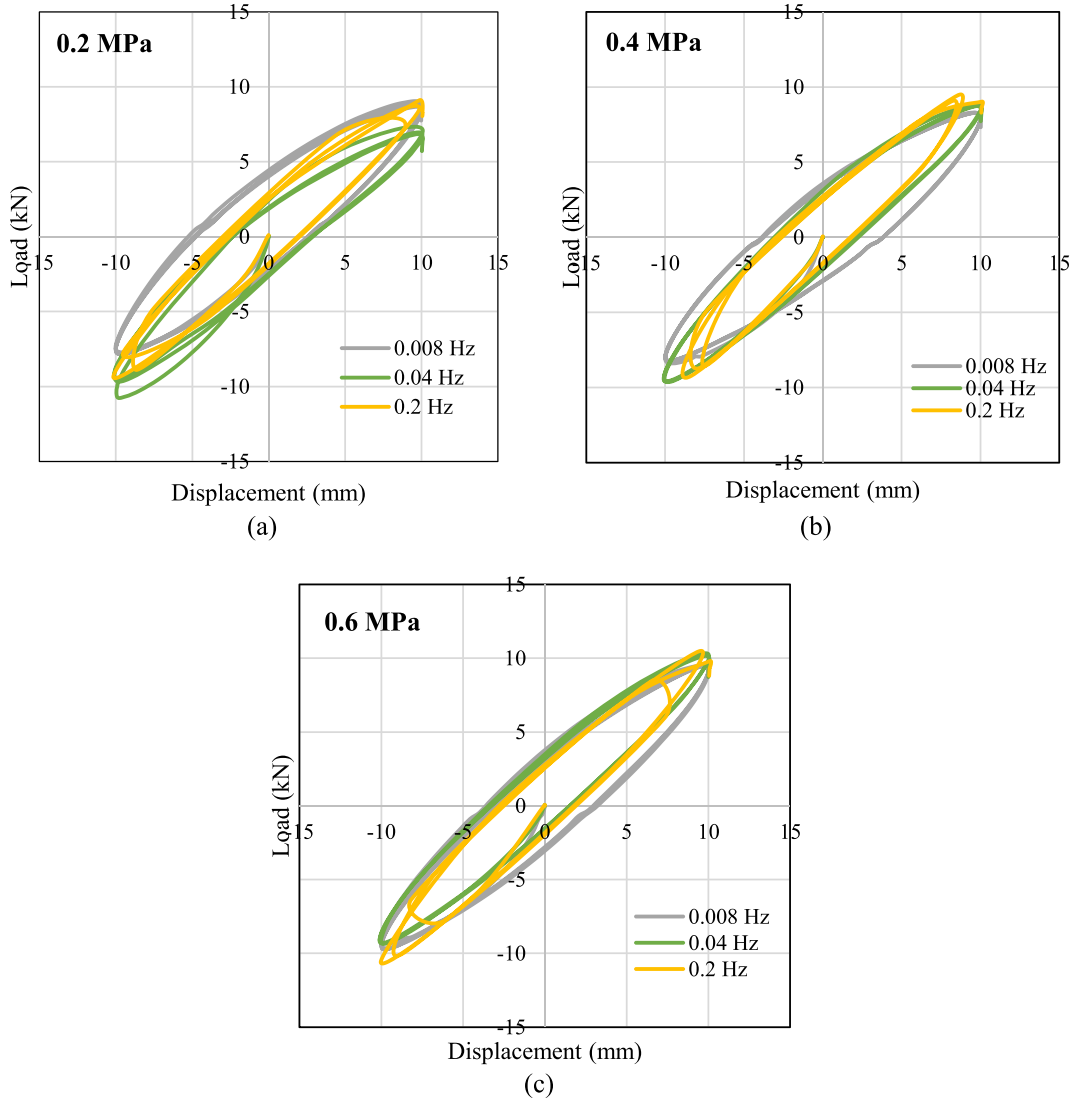

Fig. 18. Cyclic shear response of triplets with mortar-rubber joints tested under various frequencies of oscillation for different pre-compression levels: (a) 0.2 (b) 0.4 and (c) 0.6 MPa.

Table 3
Peak load of masonry triplets obtained from monotonic shear tests.

Samples	Pre-compression (MPa)	Peak stress (MPa)	
		Mortar joints	Mortar-rubber joints
1	0	–	0.12
2	0.2	0.83	0.18
3	0.4	0.94	0.21
4	0.6	1.22	0.24

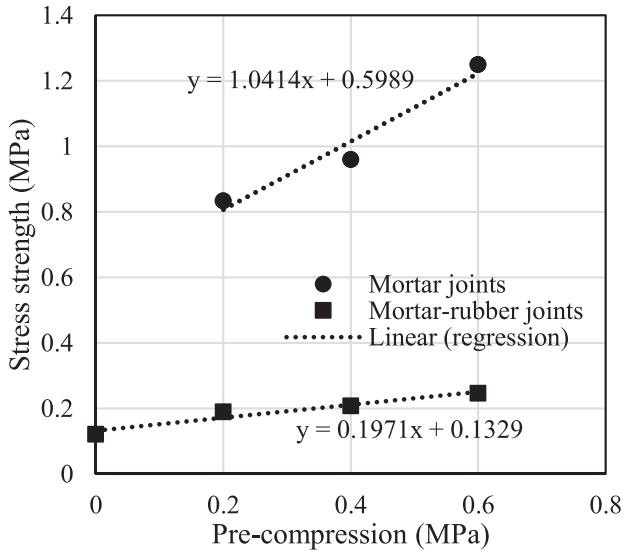

Fig. 19. Relationship between shear strength and pre-compression stress obtained by testing the triplets with mortar and mortar-rubber joints under monotonic loading.

describing the mechanical properties of the brick units, the mortar layer, and the interfaces. The last columns of Tables 4 and 5 describe the source of the values used for the parameters of the components of the triplet models. It is noteworthy that most of these values have been taken from the characterisation tests carried out on the specimens of brick and mortar. Some parameter values (e.g., the mortar tensile test and fracture energy) have been calibrated to achieve a better fit to experimental results. Nevertheless, all the parameter values are within the ranges recommended in the literature.

Fig. 20a shows the model developed for the triplets with mortar joints, using a fine mesh with element size of 10 mm. Fig. 20b shows the deformed shape of the model at failure and the plastic strain distribution, highlighting the high concentration of damage in correspondence of the mortar joints and at the interface.

Fig. 21 compares the experimental and numerical responses of the masonry triplets with mortar joints under monotonic loading at different levels of pre-compression. Two different mesh sizes were considered (with characteristic element length of 10 mm and 20 mm) without noticing significant changes in the simulated response, which is quite well described by the proposed model. In particular, the proposed model simulates with good accuracy the behaviour of the triplets up to the peak load, whereas it overestimates the post-peak stiffness of the softening branch. For the fracture energy, we assumed a value of 0.04 MPa·mm (Fig. 21e) based on the numerical analysis carried out on the model with 0.2 MPa pre-compression considering different values in a range recommended by Lourenço [36]. Similarly, a comparison between the simulations of the triplet test obtained for five different values of the tensile resistance (with a constant fracture energy of 0.04 MPa·mm). It is noteworthy that the value of 2.75 MPa (Fig. 21f) of the tensile resistance of the mortar was selected to obtain a better fit to the experimental results and it is less than the one obtained with the three-point bending test (i.e., 3.76 MPa).

3.2. *Simulation of characterization rubber material tests and cyclic tests on triplets with mortar-rubber joints*

This subsection describes the simulation and results of the uniaxial and double shear tests performed on rubber test pieces and the cyclic tests performed on triplets with mortar-rubber joint. The rubber is modelled using 3D 8-noded solid elements with a first-order hybrid formulation (C3D8H) to prevent volumetric locking, which is recommended to model the almost incompressible rubber material [51].

The pins in the rubber are not taken into account in the numerical model, and a tie constraint is introduced between the rubber joints and the mortar layers. The proposed model cannot describe the friction mechanism and the progressive degradation of the bond between the joints and the mortar up to failure. Thus, it is used here to simulate only the tests under small displacement amplitudes.

Following the approach developed by Bergstrom and Boyce [55], the

Table 4
Mechanical properties of the triplet components (brick and mortar units).

Mechanical properties	Brick units	Mortar	Source
Young's modulus, E (MPa)	18,350	1747	Material characterisation tests
Poisson's ratio, ν (-)	0.16	0.15	–
Compressive strength, σ_c (MPa)	13.53	16.47	Material characterisation tests
Strain at peak compressive stress	–	0.04	–
Peak tensile strength, σ_t (MPa)	3.75	2.75	Material characterisation tests, best fit to test results
Fracture energy in tension, G_f^I (MPa·mm)	0.07	0.04	Value within the range recommended by [36], best fit to test results

Table 5
Properties of the contact interfaces describing the brick–mortar joints.

Mortar Interaction Properties	Brick-mortar joints	Source
k_n^m per unit area (N/mm^3)	1000	Penalty parameter [44]
k_s^m, k_t^m per unit area (N/mm^3)	500	Penalty parameter [44]
σ_t(MPa)	0.14	Best fit to test results
Cohesion, c (MPa)	0.6	Triplet tests
Coefficient of friction, μ (-)	1.04	Triplet tests
Normal fracture energy per unit area, G_f^I (MPa·mm)	0.015	Value within the range recommended by [36], best fit to test results
Shear fracture energy per unit area, G_f^{II} (MPa·mm)	0.09	Value within the range recommended by [36], best fit to test results

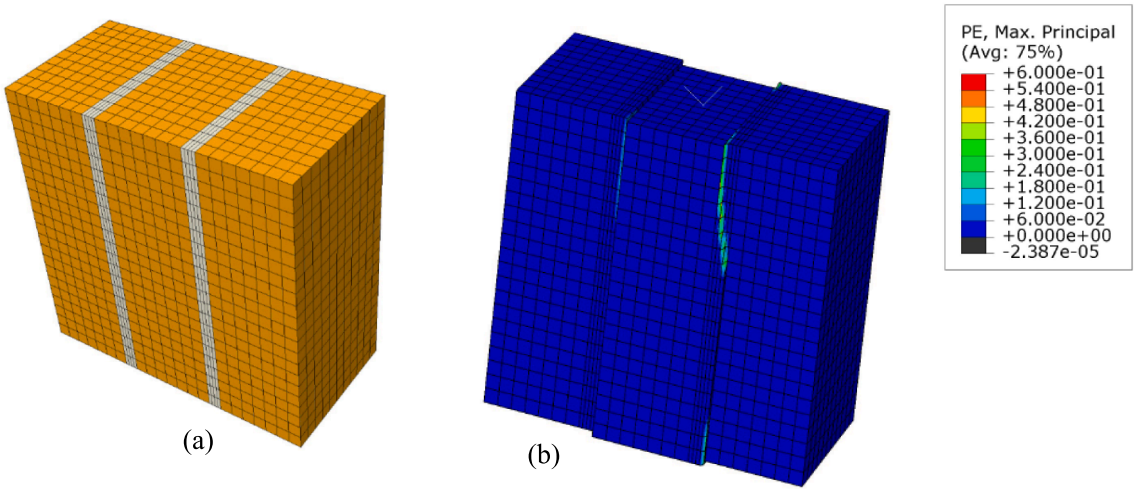

Fig. 20. (a) FE model with refined mesh (b) plastic strain distributions for mortar triplets.

mechanical response of the rubber is described by two networks working in parallel. The first one, network A, corresponds to the time-independent behaviour of the rubber, which is described by a hyperelastic model. The other, network B, describes the non-linear rate-dependent part of the response, responsible for the hysteretic behaviour.

In particular, the Yeoh model [56] is adopted for the hyperelastic component of the response, whose strain energy potential W has the following expression:

$$W = \sum_{i=1}^{3} C_{i0}(I_1 - 3)^i \tag{8}$$

where I_1 is the first invariant of strain tensor and C_{i0} are material parameters.

The Bergstrom-Boyce material model [55] is used to describe the rate-dependent hysteretic behaviour of the rubber. The strain-rate in network B is given by the following equation:

$$\dot{\varepsilon}_B = A[\lambda_B - 1]^c(\sigma_B)^m \tag{9}$$

where $\dot{\varepsilon}_B$ is the effective creep strain rate, λ_B-1 is the nominal creep strain and σ_B is the effective stress. A, m and c are material constants. A stress scaling factor S is also required, which defines the ratio of the stress carried by network B to the stress carried by network A. The total response of the model is obtained by summing the responses of the two networks.

Table 6 shows the values of the parameters of the Yeoh and Bergstrom-Boyce models, which are calibrated to provide the best fit to both the shear and the relaxation tests carried out on the quadruplets and the triplet test results for maximum shear amplitudes up to 15 mm. While different sets of parameters could be found that provide a better fit to each test results than the one considered, preference has been given to a single set of values that provide a reasonable fit to all the test results. This is expected to lead to some inaccuracies, which are however unavoidable due to the complex behaviour of the rubber joint, the limitations of the models available in Abaqus for the rubber and the cohesive bond, and the simplifications introduced in the modelling strategy (e.g. the pins in the rubber are not modelled). The development of a very sophisticated model that accurately simulates the results is out of the scope of the present study.

Fig. 22a-c compare the shear tests performed on the quadruplet with the numerical results, whereas Fig. 22d compare the shear stress–strain response and the relaxation curves of the quadruplet specimen. It can be observed that the proposed model and calibrated parameters provide a fair approximation of the complex mechanical behaviour of the rubber under different loading conditions.

Regarding the triplet numerical model, tie constraints have been adopted between the brick–mortar and mortar-rubber interfaces during cyclic tests. Fig. 23a shows the model of the masonry triplet with rubber joints. A pressure load has been applied along the z direction to simulate the initial pre-compression levels and subsequently three cycles of sinusoidal displacement are applied along the $\times$ direction while preventing translation along z and rotation of the external brick blocks.

Fig. 23b illustrates the deformed shape together with the engineering shear strain distributions of the triplet subjected to the highest pre-compression 0.6 MPa and 15 mm lateral displacement. It can be observed that the highest local shear strains are concentrated within the rubber layers. Fig. 24-Fig. 25 show the results of the numerical simulation of cyclic tests under 0.2, 0.4, and 0.6 MPa pre-compression and amplitudes of 10 and 15 mm respectively. A fair agreement can be observed between model predictions and experimental results.

The bond between the rubber layers and the mortar layers has been found to be the weakest component of the composite system in all the triplet tests carried out. Thus, future research efforts should be aimed to increase the bond resistance, in order to guarantee that the good energy dissipation capabilities of the rubber compounds are exploited, and avoid residual deformations associated with the bond failure. Alternatively, rubber layers with increased thickness could be employed to reduce the stresses at the rubber-bond interface.

4. Conclusions

This paper has presented the outcomes of an extensive experimental and numerical campaign aimed at characterising the mechanical behaviour of mortar-rubber joints used for enhancing the performance of masonry infills in reinforced concrete frames. In the first part of the paper, the experimental tests of brick, mortar and rubber are illustrated, together with cyclic shear tests of masonry triplets with mortar and mortar-rubber joints. These tests were carried out using an experimental apparatus specifically developed for the study. The second part of the paper illustrates the numerical models used for simulating the cyclic shear tests of the masonry triplets, with the material behaviour

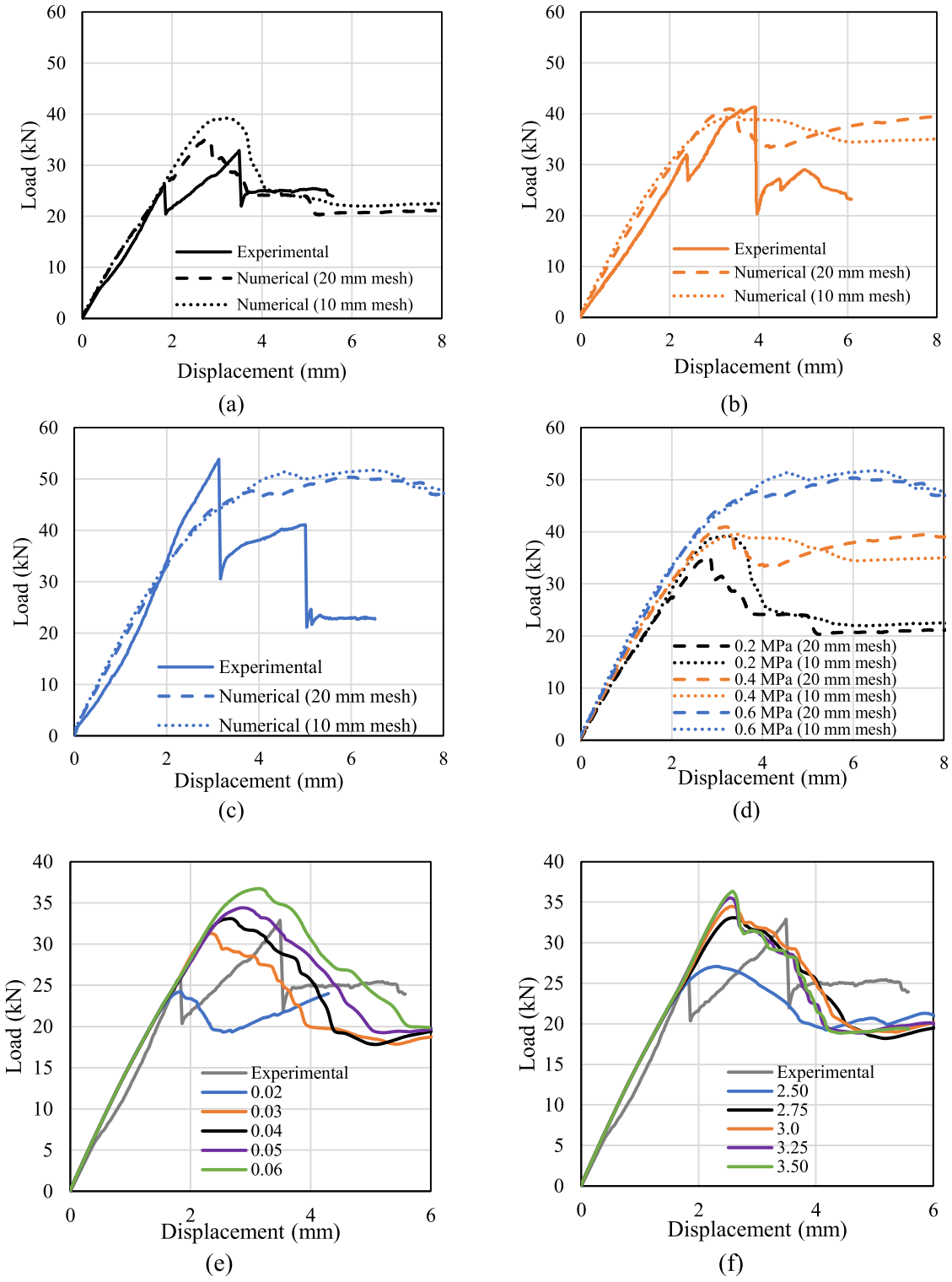

Fig. 21. (a, b, c) Comparison of experimental and numerical response of the mortar triplets under monotonic loading at (a) 0.2 MPa (b) 0.4 MPa (c) 0.6 MPa pre-compression (d) Comparison of numerical responses only (e, f) sensitivity analysis for the selected tensile strength and fracture energy of mortar.

Table 6
Material parameters of Yeoh model (MPa) and Bergstrom-Boyce model.

Yeoh model			*Bergstrom- Boyce model*			
C_{10}	C_{20}	C_{30}	S	A [$S^{-1}MPa^{-1}$]	m	c
0.112588	−0.00937779	0.000249563	1.35086	0.978683	1.48367	−0.00705511

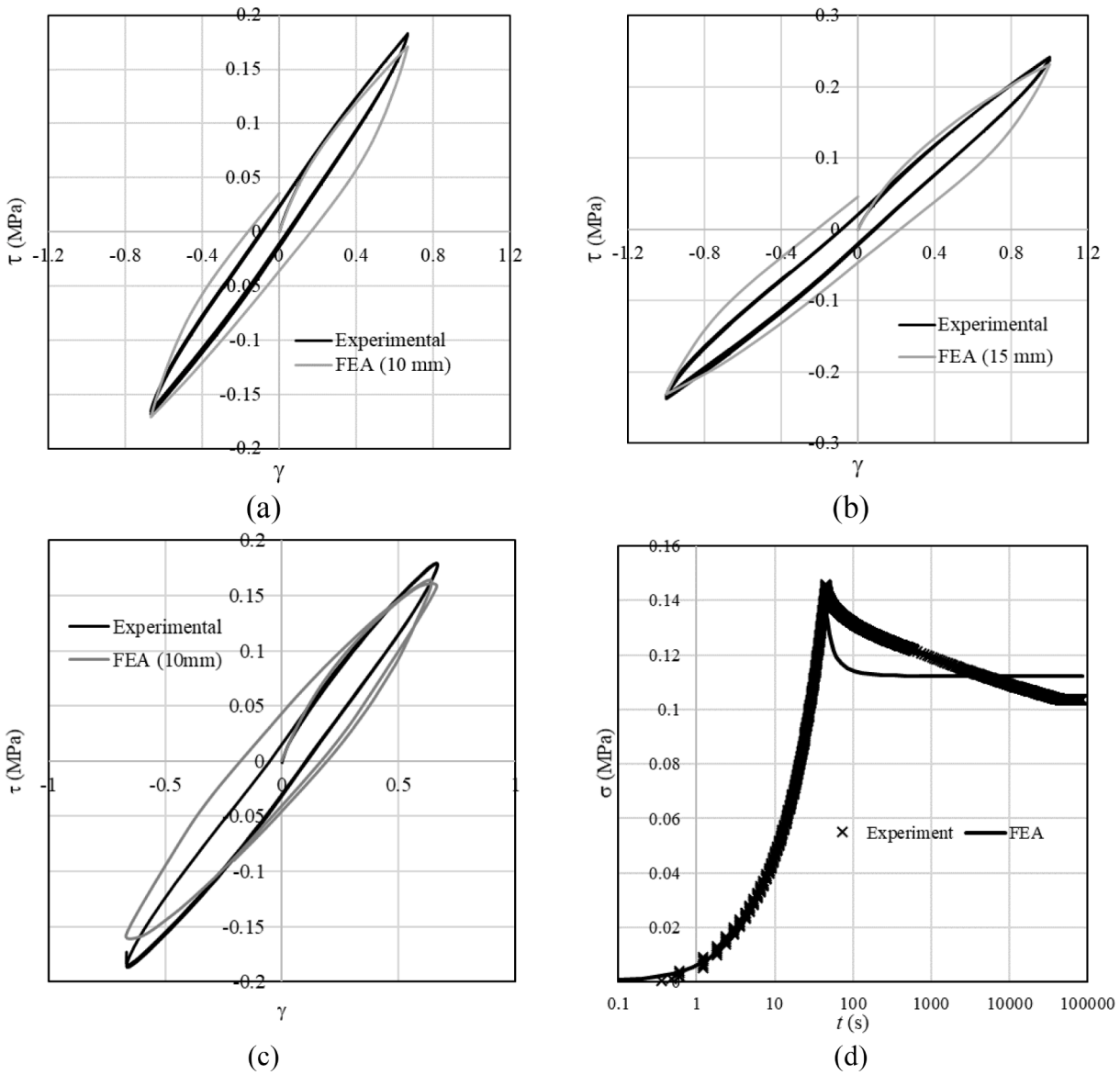

Fig. 22. Comparison of experimental and numerical shear responses of quadruplet rubber specimen: cyclic constant rate loading with maximum amplitude of (a)$\gamma = 0.67$, (b)$\gamma = 1$, (c) cyclic sinusoidal input with amplitude$\gamma = 0.67$, and (d) relaxation test at$\gamma = 0.5$.

calibrated based on the tests of brick, mortar and rubber specimens.

Based on the study results, the following conclusions can be drawn:

- The mortar-rubber joints exhibit very good dissipative properties, with an equivalent damping ratio values of the order of 20% or more which is much higher than that of the rubber compound (of the order of 6%). This is due to the frictional mechanism activated at the interface between the rubber joints and the mortar, enhanced by the presence of pins in the surface of the rubber joints.

- The measured high energy dissipation capabilities of the joints demonstrate the potential of these devices to contribute significantly to the dissipation of the seismic energy in the structures where they are inserted. This feature of the behaviour of the joints could be exploited to reduce the seismic demand in infilled reinforced concrete buildings, without requiring the use of auxiliary energy dissipation devices;

- The bond between the rubber layers and the mortar layers was found to be the weakest component of the composite system. While the failure of this bond reduces the stiffening effect of the infills, and increases even further the damping capabilities of the joints due to the activation of the frictional mechanism, it may be not desirable because it may result in residual deformations and a weakening of the infill panel in the out-of-plane direction. In order to avoid bond failure, the rubber layers should be designed to undergo shear deformations below the bond capacity, for example by increasing their thickness to limit the shear deformations they would undergo.

- The bond between the rubber joints and the mortar layers exhibited higher strengths under cyclic loading compared to monotonic loading. This phenomenon, already observed in other experimental studies on similar type of joints, should be further investigated; moreover, alternative types of rubber joints, exhibiting better bond properties, should be developed and tested.

- The proposed modelling strategy provides a fair description of the behaviour of masonry triplets with mortar-rubber joints, thanks to the use of an advanced model capable to simulate the complex amplitude- and rate-dependent behaviour of the high-damping natural rubber compound. However, further investigations need to be carried out to better understand and model the complex interaction between the rubber joints and the mortar layers. Future studies should be aimed at improving the modelling of the interaction of the rubber joint and the

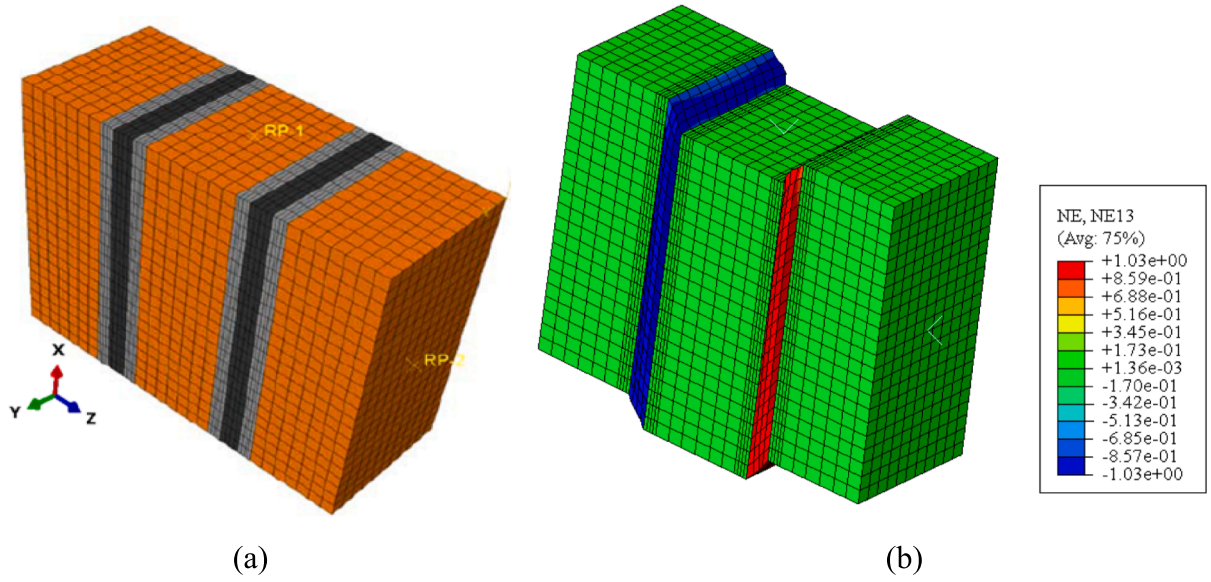

Fig. 23. (a) FE model of the masonry triplets with mortar-rubber joints, (b) nominal strain distributions for mortar-rubber triplets subjected to the maximum level of pre-compression in combination with 15 mm lateral displacement.

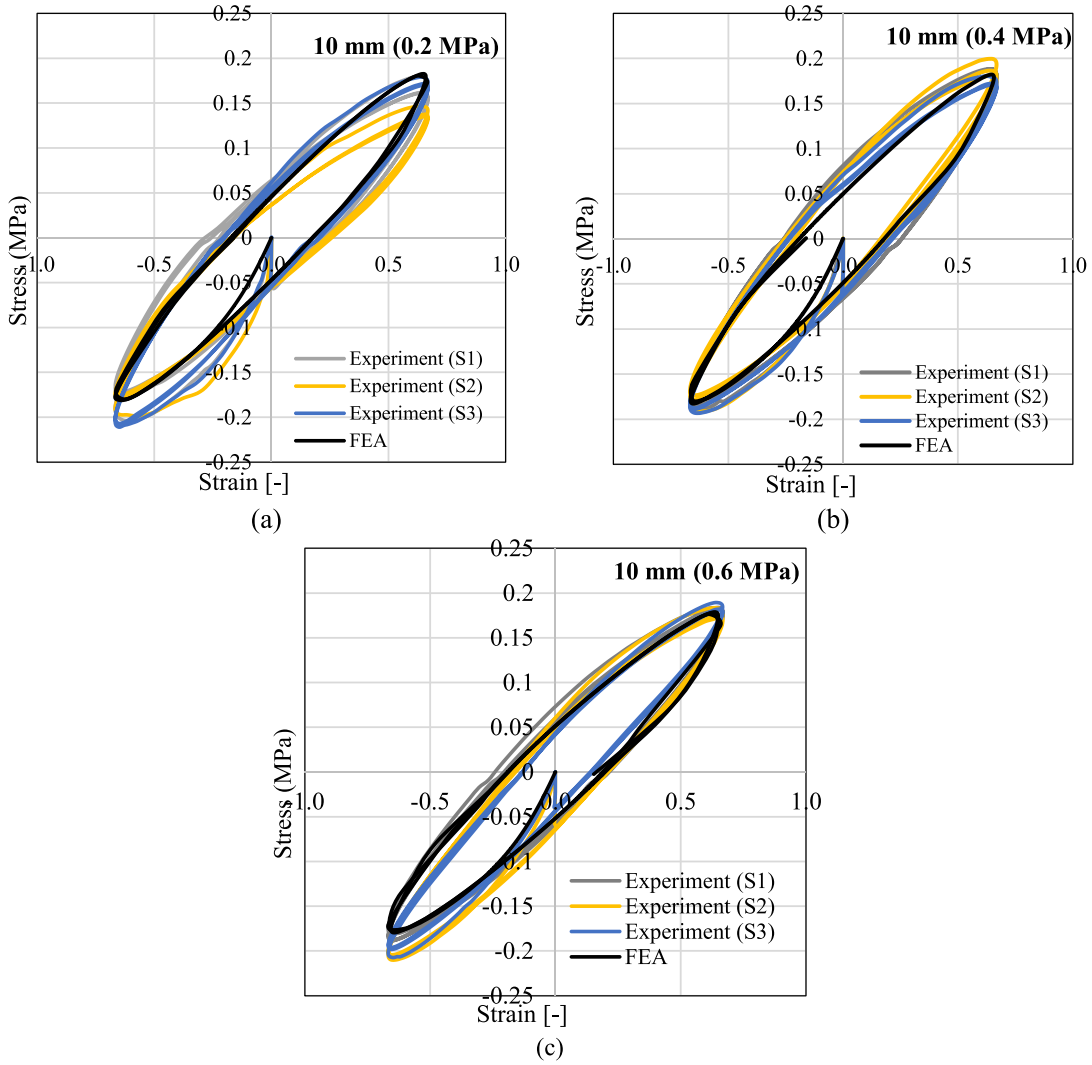

Fig. 24. Comparison of experimental and numerical cyclic shear response of the masonry triplet at 10 mm amplitude and pre-compression (a) 0.2 MPa, (b) 0.4 MPa, and (b) 0.6 MPa.

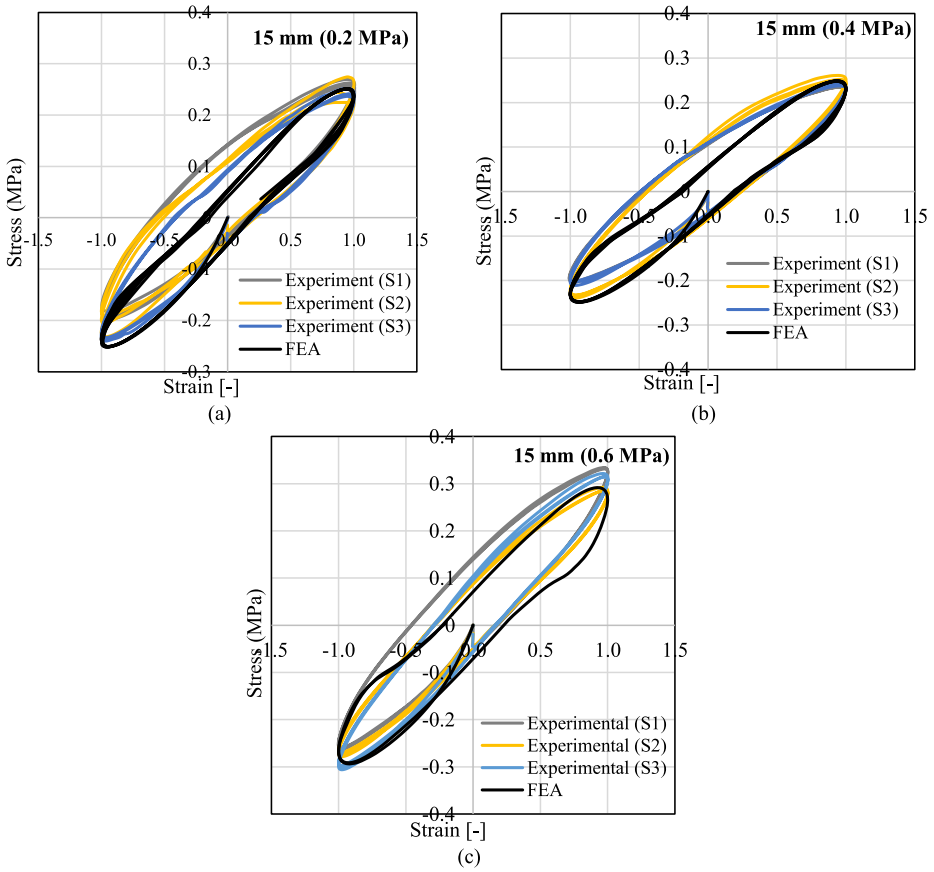

Fig. 25. Comparison of experimental and numerical cyclic shear response of the masonry triplet at 15 mm amplitude and pre-compression (a) 0.2 MPa, (b) 0.4 MPa, and (b) 0.6 MPa.

mortar layer through the pins, and at simulating the degradation and failure of the bond between the joint and the mortar.

CRediT authorship contribution statement

Prateek Kumar Dhir: Conceptualization, Methodology, Software, Data curation, Writing – original draft. **Enrico Tubaldi:** Conceptualization, Methodology, Software, Data curation, Writing – original draft, Investigation, Supervision, Visualization, Writing – review & editing. **Alessandra Orfeo:** Conceptualization, Methodology, Software. **Hamid Ahmadi:** Investigation, Supervision, Writing – review & editing.

Declaration of Competing Interest

The authors declare that they have no known competing financial interests or personal relationships that could have appeared to influence the work reported in this paper.

Acknowledgements

We are thankful to the Structural Engineering Laboratory at the University of Strathclyde and the staff (James Francis, Gavin Gibson, and Derek McNee) for the help during the experimental campaign. We would also like to thank the Earthquake Engineering Field Investigation Team (EEFIT) for their support to the experimental activity with a research grant.

References

[1] R. Villaverde, Seismic design of secondary structures: state of the art, J. Struct. Eng. 123 (8) (1997) 1011–1019, https://doi.org/10.1061/(ASCE)0733-9445(1997)123:8(1011).
[2] A. Filiatrault, T. Sullivan, Performance-based seismic design of nonstructural building components: the next frontier of earthquake engineering, Earthq. Eng. Eng. Vib. 13 (1) (2014) 17–46, https://doi.org/10.1007/s11803-014-0238-9.
[3] C. Del Vecchio, M. Di Ludovico, S. Pampanin, A. Prota, Repair costs of existing rc buildings damaged by the l'aquila earthquake and comparison with FEMA P-58 predictions, Earthq. Spectra 34 (1) (2018) 237–263, https://doi.org/10.1193/122916EQS257M.
[4] M.T. De Risi, C. Del Gaudio, G.M. Verderame, Evaluation of repair costs for masonry infills in RC buildings from observed damage data: the case-study of the 2009 L'Aquila earthquake, Buildings 9 (5) (2019), https://doi.org/10.3390/buildings9050122.
[5] V. Thiruvengadam, et al., A macro-element modelling approach of infilled frame structures, Eng. Struct. 13 (2) (2018) 327–338, https://doi.org/10.1016/j.compstruc.2014.07.008.
[6] P. Morandi, R.R. Milanesi, G. Magenes, "Innovative seismic solution for clay masonry infills with sliding joints: Principles and details," *Brick Block Mason. Trends, Innov. Challenges - Proc. 16th Int. Brick Block Mason. Conf. IBMAC 2016*, pp. 1273–1282, 2016, 10.1201/b21889-158.
[7] M. Preti, N. Bettini, G. Plizzari, Infill walls with sliding joints to limit infill-frame seismic interaction: large-scale experimental test, J. Earthq. Eng. 16 (1) (2012) 125–141, https://doi.org/10.1080/13632469.2011.579815.
[8] M. Preti, V. Bolis, A. Stavridis, Seismic infill–frame interaction of masonry walls partitioned with horizontal sliding joints: analysis and simplified modeling, J. Earthq. Eng. 23 (10) (2019) 1651–1677, https://doi.org/10.1080/13632469.2017.1387195.
[9] V. Bolis, et al., Numerical investigation of the in-plane performance of masonry-infilled RC frames with sliding subpanels, J. Earthq. Eng. 5 (2) (2019) 792–817, https://doi.org/10.1002/eqe.3163.
[10] F. Di Trapani, V. Bolis, F. Basone, M. Preti, Seismic reliability and loss assessment of RC frame structures with traditional and innovative masonry infills, Eng. Struct. 208 (February) (2020), 110306, https://doi.org/10.1016/j.engstruct.2020.110306.

[11] M. Preti, L. Migliorati, E. Giuriani, Experimental testing of engineered masonry infill walls for post-earthquake structural damage control, Bull. Earthq. Eng. 13 (7) (2015) 2029–2049, https://doi.org/10.1007/s10518-014-9701-2.

[12] C. Vögeli, N. Mojsilović, B. Stojadinović, Masonry wallettes with a soft layer bed joint: Behaviour under static-cyclic loading, Eng. Struct. 86 (2015) 16–32, https://doi.org/10.1016/j.engstruct.2014.12.038.

[13] H. Ahmadi, A. Dusi, J. Gough., "A Rubber-Based System for Damage Reduction in Infill Masonry Walls," 2017.

[14] N. Mojsilović, M. Petrović, X.R. Anglada, Masonry elements with multi-layer bed joints: behaviour under monotonic and static-cyclic shear, Constr. Build. Mater. 100 (2015) 149–162, https://doi.org/10.1016/j.conbuildmat.2015.09.065.

[15] A. Calabria, G. Guidi, F. da Porto, C. Modena, "Innovative systems for masonry infill walls based on the use of rubber joints: Finite element modelling and comparison with in-plane tests," *Brick Block Mason. Trends, Innov. Challenges - Proc. 16th Int. Brick Block Mason. Conf. IBMAC 2016*, pp. 1155–1162, 2016, 10.1201/b21889-144.

[16] M. Petrović, N. Mojsilović, B. Stojadinović, Masonry walls with a multi-layer bed joint subjected to in-plane cyclic loading: an experimental investigation, Eng. Struct. 143 (2017) 189–203, https://doi.org/10.1016/j.engstruct.2017.04.025.

[17] M. Petrović, B. Stojadinović, N. Mojsilović, I-shaped unreinforced masonry wallettes with a soft-layer bed joint: behavior under static-cyclic shear, J. Struct. Eng. 143 (11) (2017) 1–20, https://doi.org/10.1061/(ASCE)ST.1943-541X.0001884.

[18] M. Preti, B. Nicola, M. Laura, B. Valentino, S. Andreas, A.P. Giovanni, Analysis of the in-plane response of earthen masonry infill panels partitioned by sliding joints, Earthq. Eng. Struct. Dyn. 45 (8) (2016) 1209–1232.

[19] N. Verlato, Development of a Clay Masonry Enclosure System With Deformable Joints: Experimental Analysis and Numerical, Università Degli Studi Di Brescia, Italy, 2017. Doctoral dissertation.

[20] INSYSME, "INnovative SYStems for earthquake resistant Masonry Enclosures in reinforced concrete buildings," 2016. [Online]. Available: www.insysme.eu.

[21] EN 1052-3, "Methods of Test for Mortar for Masonry," *Part 3 Determ. Initial Shear strength*, vol. 3, no. 1, 2002.

[22] N. Mojsilović, M. Petrović, B. Stojadinović, Multi-layer masonry bed joint subjected to shear: analytical modelling, Constr. Build. Mater. 205 (2019) 602–610, https://doi.org/10.1016/j.conbuildmat.2019.02.051.

[23] K. Lin, H. Liu, C. Wei, Q. Huang, Effects of shear rate on cyclic behavior of dry stack masonry joint, Constr. Build. Mater. 157 (2017) 809–817, https://doi.org/10.1016/j.conbuildmat.2017.09.062.

[24] S. Barattucci, et al., An experimental and numerical study on masonry triplets subjected to monotonic and cyclic shear loadings, Constr. Build. Mater. 254 (2020), 119313, https://doi.org/10.1016/j.conbuildmat.2020.119313.

[25] S. Pietruszczak, X. Niu, A mathematical description of macroscopic behaviour of brick masonry, Int. J. Solids Struct. 29 (5) (1992) 531–546, https://doi.org/10.1016/0020-7683(92)90052-U.

[26] I. Caliò, M. Marletta, B. Pantò, A new discrete element model for the evaluation of the seismic behaviour of unreinforced masonry buildings, Eng. Struct. 40 (2012) 327–338, https://doi.org/10.1016/j.engstruct.2012.02.039.

[27] I. Caliò, B. Pantò, A macro-element modelling approach of infilled frame structures, Comput. Struct. 143 (2014) 91–107, https://doi.org/10.1016/j.compstruc.2014.07.008.

[28] W.W. El-Dakhakhni, R.G. Drysdale, M.M. Khattab, Multilaminate macromodel for concrete masonry: formulation and verification, J. Struct. Eng. 132 (12) (2006) 1984–1996, https://doi.org/10.1061/(ASCE)0733-9445(2006)132:12(1984).

[29] B. Pantò, I. Caliò, P.J.B.B. Lourenço, Seismic safety evaluation of reinforced concrete masonry infilled frames using macro modelling approach, Bull. Earthq. Eng. 15 (9) (2017) 3871–3895, https://doi.org/10.1007/s10518-017-0120-z.

[30] V. Nicoletti, D. Arezzo, S. Carbonari, F. Gara, Expeditious methodology for the estimation of infill masonry wall stiffness through in-situ dynamic tests, Constr. Build. Mater. 262 (2020), 120807, https://doi.org/10.1016/j.conbuildmat.2020.120807.

[31] G. Uva, D. Raffaele, F. Porco, A. Fiore, On the role of equivalent strut models in the seismic assessment of infilled RC buildings, Eng. Struct. 42 (2012) 83–94, https://doi.org/10.1016/j.engstruct.2012.04.005.

[32] S. Ruggieri, F. Porco, G. Uva, D. Vamvatsikos, Two frugal options to assess class fragility and seismic safety for low-rise reinforced concrete school buildings in Southern Italy, Bull. Earthq. Eng. 19 (3) (2021) 1415–1439, https://doi.org/10.1007/s10518-020-01033-5.

[33] S. Ruggieri, F. Porco, G. Uva, A Practical Approach for Estimating the Floor Deformability in Existing RC Buildings: Evaluation of the Effects in the Structural Response and Seismic Fragility, vol. 18, no. 5, Springer, Netherlands, 2020.

[34] A. Mohyeddin, H.M. Goldsworthy, E.F. Gad, FE modelling of RC frames with masonry infill panels under in-plane and out-of-plane loading, Eng. Struct. 51 (2013) 73–87, https://doi.org/10.1016/j.engstruct.2013.01.012.

[35] K.F. Abdulla, L.S. Cunningham, M. Gillie, Simulating masonry wall behaviour using a simplified micro-model approach, Eng. Struct. 151 (2017) 349–365, https://doi.org/10.1016/j.engstruct.2017.08.021.

[36] P.J.B.B. Lourenço, Computational strategies for masonry structures, Delft University of Technology, Holland, 1997. Doctoral dissertation.

[37] V. Sarhosis, K.D. Tsavdaridis, I. Giannopoulos, Discrete element modelling of masonry infilled steel frames with multiple window openings subjected to lateral load variations, Open Constr. Build. Technol. J. 8 (1) (2014) 93–103, https://doi.org/10.2174/1874836801408010093.

[38] P.B. Lourenço, J.G. Rots, Multisurface interface model for analysis of masonry structures, J. Eng. Mech. 123 (7) (1997) 660–668, https://doi.org/10.1061/(ASCE)0733-9399(1997)123:7(660).

[39] K.M. Dolatshahi, A.J. Aref, Two-dimensional computational framework of meso-scale rigid and line interface elements for masonry structures, Eng. Struct. 33 (12) (2011) 3657–3667, https://doi.org/10.1016/j.engstruct.2011.07.030.

[40] L. Macorini, B. Izzuddin, A non-linear interface element for 3D mesoscale analysis of brick-masonry structures, Int. J. Numer. Methods Eng. 85 (12) (2011) 1584–1608.

[41] L. Macorini, B.A. Izzuddin, Nonlinear analysis of masonry structures using mesoscale partitioned modelling, Adv. Eng. Softw. 60–61 (2013) 58–69, https://doi.org/10.1016/j.advengsoft.2012.11.008.

[42] L. Macorini, B.A. Izzuddin, Nonlinear analysis of unreinforced masonry walls under blast loading using Mesoscale partitioned modeling, J. Struct. Eng. 140 (8) (2014) 1–10, https://doi.org/10.1061/(ASCE)ST.1943-541X.0000931.

[43] E. Nasiri, Y. Liu, Development of a detailed 3D FE model for analysis of the in-plane behaviour of masonry infilled concrete frames, Eng. Struct. 143 (2017) 603–616, https://doi.org/10.1016/j.engstruct.2017.04.049.

[44] P.K. Dhir, E. Tubaldi, H. Ahmadi, J. Gough, Numerical modelling of reinforced concrete frames with masonry infill and rubber joints, Eng. Struct. 246 (July) (2021), 112833, https://doi.org/10.1016/j.engstruct.2021.112833.

[45] EN 1015-11, "Methods of Test for Mortar for Masonry," *Part 11 Determ. Flexural Compressive Strength Hardened Mortar*, vol. 3, no. 1, 2006.

[46] Tinius Olsen, "Electromechanical Universal Testing Machines (ST Series)," 2021. https://www.tiniusolsen.com/wp-content/uploads/2021/05/ST0000EN03-ST-Series-Tester-A4.pdf.

[47] E. Tubaldi, L. Ragni, A.D. Asta, H. Ahmadi, A. Muhr, Stress softening behaviour of HDNR bearings: modelling and influence on the seismic response of isolated structures, Earthq. Eng. Struct. Dyn. 46 (12) (2017) 2033–2054, https://doi.org/10.1002/eqe.

[48] V. Alecci, M. Fagone, T. Rotunno, M. De Stefano, Shear strength of brick masonry walls assembled with different types of mortar, Constr. Build. Mater. 40 (2013) 1038–1045, https://doi.org/10.1016/j.conbuildmat.2012.11.107.

[49] G. Andreotti, F. Graziotti, G. Magenes, Detailed micro-modelling of the direct shear tests of brick masonry specimens: the role of dilatancy, Eng. Struct. 168 (May) (2018) 929–949, https://doi.org/10.1016/j.engstruct.2018.05.019.

[50] E. Franzoni, C. Gentilini, G. Graziani, S. Bandini, Towards the assessment of the shear behaviour of masonry in on-site conditions: a study on dry and salt/water conditioned brick masonry triplets, Constr. Build. Mater. 65 (2014) 405–416, https://doi.org/10.1016/j.conbuildmat.2014.05.002.

[51] D. Systèmes, "Abaqus," *RI: Dassault Systèmes*, 2016. http://www.3ds.com/products-services/simulia/products/abaqus/.

[52] J.G. Rots, *Structural masonry: An experimental/numerical basis for practical design rules*. TNO Building and Construction Research,Rijswijk, Netherlands: Centre of Civil Engineering Research and Codes (CUR), 1997.

[53] J. Lee, G.L. Fenves, A plastic-damage concrete model for earthquake analysis of dams, Earthq. Eng. Struct. Dyn. 27 (9) (1998) 937–956, https://doi.org/10.1002/(SICI)1096-9845(199809)27:9<937::AID-EQE764>3.0.CO;2-5.

[54] "Concrete damaged plasticity," *Abaqus manual*, 2017. https://abaqus-docs.mit.edu/2017/English/SIMACAEMATRefMap/simamat-c-concretedamaged.htm.

[55] J.S. Bergström, M.C. Boyce, Constitutive modeling of the large strain time-dependent behavior of elastomers, J. Mech. Phys. Solids 46 (5) (1998) 931–954, https://doi.org/10.1016/S0022-5096(97)00075-6.

[56] O. Yeoh, Some forms of the strain energy function for rubber, *Rubber Chem. Technol.* 66 (1993) 754–771, https://doi.org/10.1080/00033799300200371.